Short pulse laser propagation in underdense plasmas

M. D. Feit and J. C. Garrison
Lawrence Livermore National Laboratory, University of California, Livermore, California 94550

A. M. Rubenchik
Department of Applied Science, University of California, Davis/Livermore, California 94550
(Received 15 May 1995; revised manuscript received 1 September 1995)

Propagation of an intense laser pulse in an underdense plasma is modeled by treating the electrons as a cold relativistic fluid. For sufficiently short pulses, the ion motion is negligible. The disparities between the optical, plasma, and propagation length scales are dealt with by using a multiple scales technique to derive approximate equations averaged over successively larger length scales. This argument does not require the quasistatic approximation (QSA) often used in earlier works, and it shows that, in the coordinate system moving with the pulse, the fluid will exhibit transient temporal oscillations. Asymptotically, i.e., for times that are long on the plasma scale, the transient solution approaches the QSA. The problem of matching the transient (inner) solution to the asymptotic (outer) solution is solved by means of a uniformly valid, two-time expansion. The QSA is shown to suffer from instabilities, which could cause serious problems for numerical simulations of long pulses, and an "improved-QSA," suggested by the inner-outer analysis, is demonstrated. An analytical solution for a planar, weak-field model is presented that explicitly displays the transient behavior of the fluid. For a short, cylindrically symmetric, weak-field pulse, numerical simulations that include relativistic self-focusing, forward Raman scattering, and ponderomotive forces show the importance of the transient effects in a more realistic case.

PACS number(s): 52.40.Nk, 42.65.Jx, 52.35.Mw

I. INTRODUCTION

The fast igniter concept [1] for inertial confinement fusion has produced a new surge of interest in the propagation of intense ($I > 10^{17}$ W/cm^2) laser pulses in underdense plasmas. This problem has been studied for some time in connection with laser acceleration of particles [2]. The two applications differ mainly in emphasis; the propagation of the strong pulse itself is the main point of interest for the fast igniter application, whereas the plasma waves generated in the wake of the main pulse are the important phenomenon for laser wake-field acceleration. At these very high intensities, the propagation of the pulse and the generation of wake fields are highly nonlinear phenomena. The standard analytical techniques used in the study of linear propagation are therefore of little use, and numerical simulation is required.

The general nonlinear propagation problem has been extensively studied by means of particle simulations [3-5]. In principle, this method can include all the relevant physics exactly, but the simulations are memory intensive and long running. As a consequence of this practical limitation most fundamental calculations are restricted to one transverse dimension, and even these restricted computations are still very time consuming. Since self-focusing singularities are different in one and two transverse dimensions, it is clearly essential to study the influence of dimensionality. In addition to this fundamental issue, the design and interpretation of experiments requires exploration of the parameter space. For this purpose it is very desirable to have a suite of programs that require smaller computational resources. After these approximate simulations have located the appropriate small range of parameters, more exact particle simulations could be used to perform the final optimization.

The fluid model of the plasma that we use in this paper has also been extensively employed in previous propagation studies [6-13], and it is much less computationally demanding than particle simulations. The most basic feature of propagation in underdense plasmas is that the laser wavelength is small compared to the plasma wavelength, which is in turn small compared to the diffraction length. The presence of large ratios among the fundamental length scales leads to "stiff" differential equations [14], both in the particle and fluid simulations. Stiff equations require special numerical methods, but there are analytical techniques for which the disparity of length scales is an advantage. These approaches, which include the method of averages [15], multiple time scales [16], and the renormalization group [17], are well known in nonlinear optics [18] and plasma physics [19]. In the present paper, we have carried out a multiple-scales analysis of the combined Maxwell and relativistic fluid equations. In this procedure the optical length and time scales are explicitly eliminated, and phenomena occurring on the plasma and diffraction scales are treated by a two-variable expansion [20]. The approximate equations obtained in this way are similar to those used in earlier work [9], but our analysis provides a clear and explicit derivation that shows that the equations represent the leading order in a systematic expansion scheme. Furthermore, essentially all existing applications of these equations also make the well-known quasistatic approximation (QSA) [21,22]. In the QSA, the electron fluid is assumed to be stationary in the frame of reference moving

with the pulse; there is no independent plasma dynamics. In this approximation the fluid variables cannot satisfy the initial conditions, e.g., quiescent plasma, which are physically required. Thus a complete description requires some way of connecting the initial conditions to the QSA. In our analysis, the higher-order time derivatives are multiplied by the small parameter of the expansion. This feature is known to produce solutions that display boundary layer behavior [20]. In our case the variable is time, so we will refer to the boundary layer as the initial layer. Our analysis shows that there are transient oscillations in the plasma that asymptotically approach the QSA result. For sufficiently large propagation lengths, this initial transient behavior may not be important, but experiments involving thin plasmas should reveal significant deviations from the QSA.

In this paper the laser pulse duration is assumed to be short enough to allow the neglect of ion motions, and the intensity high enough to drive the electrons to velocities large compared to their thermal velocities in a few optical periods. Under these circumstances the electrons can be treated as a cold relativistic fluid. In a later paper we will treat intense long pulses for which significant ion motion is involved. For a typical laser wavelength of 1 μm, the critical density is about $N_c = 10^{21}$ cm^{-3}, and a pulse intensity of the order 10^{17} W/cm^2 will produce a quiver energy of order 20 keV, which is large compared to the plasma temperatures expected in current experiments. The dynamical response of the electron fluid can be followed in three dimensions, but we will initially assume cylindrical symmetry in order to decrease the computational costs. The fluid equations, together with the assumption of paraxial propagation for the laser pulse, will allow us to treat diffraction, ponderomotive effects, and relativistic self-focusing.

In Sec. II we present the exact dynamical equations for the fluid model and discuss the choice of appropriate normalizations. The slowly varying envelope approximation is used in Sec. III to separate the optical frequency oscillations of the laser carrier wave from the plasma response, and in Sec. IV we derive a uniformly valid expansion of the field and the fluid variables in the small parameter $\theta = \sqrt{N_e/N_c}$. We use the leading order in this expansion to show the existence of transient oscillations in the fluid variables that asymptotically approach the quasistatic form, which has been frequently used in earlier work [9]. The transient behavior is interpreted in terms the inner and outer solutions employed in the analysis of boundary layers. In Sec. V we present the fully relativistic model and exhibit the instabilities of plane-wave solutions in the quasistatic approximation. The case of weak fields, for which the electron motion is weakly relativistic, is studied in Sec. VI, and exact solutions for a one-dimensional (1D) version are used to demonstrate explicitly the approach of the initially quiescent fluid to the quasistatic limit. In this context we also use the boundary layer analysis to construct an improved numerical scheme that alleviates some of the stability problems associated with the quasistatic approximation. In Sec. VII the improved QSA is used in simulations that display the interplay between diffraction, relativistic self-focusing, and wake-field generation. Two additional simplified models, which are valid for arbitrary field strengths, are briefly discussed in Sec. VIII and Sec. IX presents a summary and conclusions.

II. THE FLUID MODEL

Under the assumptions discussed above, the dynamical equations are Maxwell's equation for the total electromagnetic field and the relativistic fluid equations for the electrons:

$$\nabla\cdot\mathbf{A}=0 \quad \text{(gauge choice)}\,, \tag{2.1}$$

$$\left[\nabla^2-\frac{1}{c^2}\partial_t^2\right]\mathbf{A}=\frac{4\pi}{c}eN_e\mathbf{v}+\frac{1}{c}\nabla\partial_t\Phi\,, \tag{2.2}$$

$$\nabla^2\Phi=-4\pi[-eN_e+eN_0n_i(\mathbf{r})]\,, \tag{2.3}$$

$$\partial_t\mathbf{P}+(\mathbf{v}\cdot\nabla)\mathbf{P}=e\nabla\Phi+\frac{e}{c}\partial_t\mathbf{A}-\frac{e}{c}\mathbf{v}\times(\nabla\times\mathbf{A})\,, \tag{2.4}$$

$$\partial_t N_e+\nabla\cdot(N_e\mathbf{v})=0\,, \tag{2.5}$$

where $\partial_t\equiv\partial/\partial t$, $\mathbf{A}$ and Φ are, respectively, the vector and scalar potentials, $\mathbf{P}=m_0\gamma\mathbf{v}$ is the electron momentum, $N(\mathbf{r},t)$ is the electron density, N_0 is the mean density, and $n_i(\mathbf{r})$ is the density profile of the ions. The force equation (2.4) can be cast into the equivalent form

$$\partial_t\left[\mathbf{P}-\frac{e}{c}\mathbf{A}\right]-\mathbf{v}\times\left[\nabla\times\left[\mathbf{P}-\frac{e}{c}\mathbf{A}\right]\right]=e\nabla\Phi-m_0c^2\nabla\gamma\,, \tag{2.6}$$

with the immediate consequence that the "vorticity" $\Omega\equiv\nabla\times(\mathbf{P}-(e/c)\mathbf{A})$ is conserved [9,12]. The initial conditions for our problem, a quiescent plasma and no field, guarantee the initial absence of vorticity; therefore the vorticity vanishes at all later times. This simplifies (2.6) to [9,12]

$$\partial_t\left[\mathbf{P}-\frac{e}{c}\mathbf{A}\right]=e\nabla\Phi-m_0c^2\nabla\gamma\,. \tag{2.7}$$

Since our primary purpose is to study the propagation of the laser pulse, we use the so-called "pulse" variables [9] defined by

$$Z=z-ct\,,\quad Z^0=ct\,,\quad \partial_z=\partial_Z\,,\quad \frac{1}{c}\partial_t=\partial_{Z^0}-\partial_Z\,. \tag{2.8}$$

The normalized equations for the fluid model are then

$$\nabla\cdot\mathbf{a}=0\,, \tag{2.9}$$

$$(\nabla_\perp^2+2\partial_{Z^0}\partial_Z-\partial_{Z^0}^2)\mathbf{a}=k_p^2\eta\mathbf{p}+\nabla(\partial_{Z^0}-\partial_Z)\phi\,, \tag{2.10}$$

$$(\nabla_\perp^2+\partial_Z^2)\phi=k_P^2(\gamma\eta-n_i)\,, \tag{2.11}$$

$$(\partial_{Z^0}-\partial_Z)(\mathbf{p}-\mathbf{a})=\nabla(\phi-\gamma)\,, \tag{2.12}$$

$$(\partial_{Z^0}-\partial_Z)(\eta\gamma)+\nabla\cdot(\eta\mathbf{p})=0\,, \tag{2.13}$$

$$\gamma=\sqrt{1+p^2}\,, \tag{2.14}$$

where $\omega_P^2=4\pi N_0e^2/m$ (plasma frequency), $k_P=\omega_P/c$ (plasma wave number), $\mathbf{p}\equiv\mathbf{P}_e/(m_0c)$ (electron momen-

tum), $\eta \equiv N_e/(\gamma N_0)$ (proper electron density), $\phi \equiv e\Phi/(m_0c^2)$ (scalar potential), and $\mathbf{a} \equiv e\mathbf{A}/(m_0c^2)$ (vector potential). For 1-μm radiation the normalized vector potential is $|\mathbf{a}|=1$ for an intensity $I=1.73\times10^{18}$ W/cm^2.

The dynamical response of the plasma is characterized by the plasma frequency ω_P, and the initial Z^0 dependence of the entering pulse is characterized by the Rayleigh range corresponding to the transverse pulse width. Since the plasma response may lead to transverse inhomogeneities of order k_P^{-1}, and typical pulse widths are larger than k_P^{-1}, the safest assumption is that the subsequent evolution of the pulse is characterized by the Rayleigh range corresponding to the width k_P^{-1}, i.e., $L_R = kk_P^{-2}$, where k is the central wave number of the pulse. The Z dependence of the incident pulse is characterized by the pulse length $L_p = cT_p$. For a nominal plasma density $N_e = 10^{20}$ cm^{-3}, a pulse width $L_p \approx k_P^{-1}$ corresponds to a pulse duration $T_p \approx 2$ fs. Such ultrashort pulses are not currently of interest, so it is safe to assume that $L_p > k_p^{-1}$. Since the incident pulse envelope can be modulated by the plasma response, the appropriate characteristic length for measuring the pulse variable Z, as well as the transverse coordinates $\mathbf{x}_\perp$, is k_p^{-1}. This suggests the use of dimensionless coordinates, ζ, $\mathbf{r}_\perp$, and T, defined by

$$\zeta = k_P Z \ , \quad \mathbf{r}_\perp = k_P \mathbf{x}_\perp \ , \quad T = Z^0/L_R \ . \tag{2.15}$$

Rewriting Eqs. (2.9)–(2.14) in these variables introduces the dimensionless parameter

$$\theta = \frac{k_P^{-1}}{L_R} = \frac{k_P}{k} = \frac{\omega_P}{\omega} = \left[\frac{N_0}{N_c}\right]^{1/2} , \tag{2.16}$$

which is the characteristic diffraction angle for an effective transverse aperture width k_P^{-1}. For underdense plasmas θ is the small parameter of the theory. The dimensionless equations are

$$\nabla\cdot\mathbf{a}=0 \ , \tag{2.17}$$

$$(\nabla_\perp^2 + 2\theta\partial_T\partial_\zeta - \theta^2\partial_T^2)\mathbf{a} = \eta\mathbf{p} + \theta\nabla\partial_T\phi - \nabla\partial_\zeta\phi \ , \tag{2.18}$$

$$\nabla^2\phi = \gamma\eta - n_i \ , \tag{2.19}$$

$$(\theta\partial_T - \partial_\zeta)(\mathbf{p}-\mathbf{a}) = \nabla(\phi-\gamma) \ , \tag{2.20}$$

$$(\theta\partial_T - \partial_\zeta)(\eta\gamma) + \nabla\cdot(\eta\mathbf{p}) = 0 \ , \tag{2.21}$$

$$\gamma = \sqrt{1+p^2} \ , \tag{2.22}$$

where $\nabla = \nabla_\perp + \hat{\mathbf{z}}\partial_\zeta$.

The interplay between phenomena occurring on the propagation scale L_R and the plasma response scale $1/k_P$ is complicated by the optical scale oscillations of the carrier wave. In the next section, we will separate out the optical scale behavior by means of the slowly varying envelope approximation (SVEA), and in subsequent sections deal with the remaining length scales.

III. THE SLOWLY VARYING ENVELOPE APPROXIMATION

The rapid optical oscillations can be treated by defining a dimensionless "fast" coordinate χ:

$$\chi = kz - \omega t = kZ = \frac{k}{k_P}\zeta = \frac{\zeta}{\theta} \ , \tag{3.1}$$

and imposing a strong form of the SVEA by the ansatz

$$X(\mathbf{r}_\perp,\zeta,T,\chi) = X_0(\mathbf{r}_\perp,\zeta,T) + X_f(\mathbf{r}_\perp,\zeta,T,\chi) \ ,$$

$$X_f(\mathbf{r}_\perp,\zeta,T,\chi) = \tfrac{1}{2}\sum_{m=-\infty}^{\infty}{}' X_m(\mathbf{r}_\perp,\zeta,T)e^{im\chi} \ ,$$

$$X_m(\mathbf{r}_\perp,\zeta,T) = X^*_{-m}(\mathbf{r}_\perp,\zeta,T) \ , \tag{3.2}$$

where X represents any of the dynamical variables. The primed sum indicates the omission of the $m=0$ term, or equivalently

$$X_f(\mathbf{r}_\perp,\zeta,T,\chi) = \mathrm{Re}\sum_{m=1}^{\infty} X_m(\mathbf{r}_\perp,\zeta,T)e^{im\chi} \ . \tag{3.3}$$

This ansatz ignores counterpropagating modes, but does allow for harmonics of the fundamental laser frequency. Using (3.2) and the chain rule substitution

$$\partial_\zeta \rightarrow \partial_\zeta + \frac{1}{\theta}\partial_\chi \ , \tag{3.4}$$

in the dynamical equations (2.17)–(2.22) yields an infinite set of equations for the Fourier components of the dynamical variables. These equations describe the evolution of the laser fundamental and its harmonics in interaction with the corresponding Fourier components of the material polarization. Since harmonics are not present in the injected pulse, they can only appear through beating of the laser fundamental with the fundamental of the polarization. Therefore the harmonics will remain small, and they will not significantly affect the evolution of the fundamental. Thus it is a good approximation to neglect all higher harmonics, i.e., all Fourier components, X_m, with $|m|>1$ are dropped. This reduces the dynamical equations to a finite set.

The $m=0$ (slow) equations are

$$\nabla\cdot\mathbf{a}_0=0 \ , \tag{3.5}$$

$$(\nabla_\perp^2 + 2\theta\partial_T\partial_\zeta - \theta^2\partial_T^2)\mathbf{a}_0 = [\eta\mathbf{p}]_0 + \theta\nabla\partial_T\phi_0 - \nabla\partial_\zeta\phi_0 \ , \tag{3.6}$$

$$\nabla^2\phi_0 = [\gamma\eta]_0 - n_i \ , \tag{3.7}$$

$$(\theta\partial_T - \partial_\zeta)(\mathbf{p}_0 - \mathbf{a}_0) = \nabla(\phi_0 - \gamma_0) \ , \tag{3.8}$$

$$(\theta\partial_T - \partial_\zeta)[\eta\gamma]_0 + \nabla\cdot[\eta\mathbf{p}]_0 = 0 \ , \tag{3.9}$$

$$\gamma_0^2 = 1 + p_0^2 + \tfrac{1}{2}\mathbf{p}_1^*\cdot\mathbf{p}_1 - \tfrac{1}{2}|\gamma_1|^2 \ , \tag{3.10}$$

where

$$[XY]_0 = X_0Y_0 + \tfrac{1}{2}\mathrm{Re}\sum_{m=1}^{\infty} X_mY_{-m} \ , \tag{3.11}$$

$$[XY]_m = X_0Y_m + X_mY_0 + \tfrac{1}{2}\sum_{n\neq m}{}' X_{m-n}Y_n \ , \quad m\neq 0 \ . \tag{3.12}$$

The $m=\pm1$ (fast) equations are

$$a_{z1}=\theta\nabla\cdot\mathbf{a}_1 , \tag{3.13}$$

$$(\nabla_\perp^2+2i\partial_T+2\theta\partial_T\partial_\xi-\theta^2\partial_T^2)\mathbf{a}_{\perp 1}=-\frac{i}{\theta}\nabla_\perp\phi_1+[\eta\mathbf{p}_\perp]_1+\theta\nabla_\perp\partial_T\phi_1-\nabla_\perp\partial_\xi\phi_1 , \tag{3.14}$$

$$(\nabla_\perp^2+2i\partial_T+2\theta\partial_T\partial_\xi-\theta^2\partial_T^2)a_{z1}=\frac{1}{\theta^2}\phi_1+[\eta p_z]_1+\theta\partial_\xi\partial_T\phi_1-\frac{2i}{\theta}\partial_\xi\phi_1+i\partial_T\phi_1-\partial_\xi^2\phi_1 , \tag{3.15}$$

$$-\phi_1+2i\theta\partial_\xi\phi_1+\theta^2\nabla^2\phi_1=\theta^2[\gamma\eta]_1 , \tag{3.16}$$

$$(\theta\partial_T-\partial_\xi)(\mathbf{p}_{\perp 1}-\mathbf{a}_{\perp 1})-\frac{i}{\theta}(\mathbf{p}_{\perp 1}-\mathbf{a}_{\perp 1})=\nabla_\perp(\phi_1-\gamma_1) , \tag{3.17}$$

$$(\theta\partial_T-\partial_\xi)(p_{z1}-a_{z1})-\frac{i}{\theta}(p_{z1}-a_{z1})=\partial_\xi(\phi_1-\gamma_1)+\frac{i}{\theta}(\phi_1-\gamma_1) , \tag{3.18}$$

$$\left[\theta\partial_T-\partial_\xi-\frac{i}{\theta}\right][\eta\gamma]_1+\nabla\cdot[\eta\mathbf{p}]_1+\frac{i}{\theta}[\eta p_z]_1=0 , \tag{3.19}$$

$$\gamma_1=\frac{\mathbf{p}_0\cdot\mathbf{p}_1}{\gamma_0} . \tag{3.20}$$

IV. TWO-VARIABLE EXPANSION

Our next task is to disentangle the plasma-scale and propagation-scale behaviors. We first present a straightforward formal procedure to accomplish this end, and then give a more detailed justification by relating our procedure to the method of matched asymptotic expansions. The formal procedure begins with the introduction of a second time scaling by $\tau=k_pZ^0=k_pL_RT=T/\theta$. A two-variable expansion scheme ([20], p. 115) is implemented by treating T and τ as independent variables and using the chain rule substitution

$$\partial_T\rightarrow\partial_T+\frac{1}{\theta}\partial_\tau , \tag{4.1}$$

in (3.5)–(3.20). Each Fourier amplitude X_m is then expanded as

$$X_m(\mathbf{r}_\perp,\xi,T,\tau)=\sum_{n=0}^{\infty}\theta^nX_m^{(n)}(\mathbf{r}_\perp,\xi,T,\tau) , \tag{4.2}$$

and the coefficients of equal powers of θ are equated. Eliminating the negative powers of θ in the fast equations (3.13)–(3.20) yields

$$\phi_1^{(0)}=a_{z1}^{(0)}=0 , \tag{4.3}$$

$$\eta_1^{(0)}=0 , \tag{4.4}$$

$$\mathbf{p}_{\perp 1}^{(0)}=\mathbf{a}_{\perp 1}^{(0)} \text{ (definition of quiver velocity)} , \tag{4.5}$$

$$\gamma_1^{(0)}=p_{z1}^{(0)} , \tag{4.6}$$

$$\partial_\tau\mathbf{a}_{\perp 1}^{(0)}=0 , \tag{4.7}$$

and all that remains is the modified paraxial wave equation:

$$(\nabla_\perp^2+2i\partial_T)\mathbf{a}_{\perp 1}^{(0)}+2i\partial_\tau\mathbf{a}_{\perp 1}^{(1)}=\eta_0^{(0)}\mathbf{a}_{\perp 1}^{(0)} . \tag{4.8}$$

The first-order amplitude $\mathbf{a}_{\perp 1}^{(1)}$ in (4.8) can be eliminated by carrying out a long-time average over the plasma-scale variable τ, and using the τ independence of $\mathbf{a}_{\perp 1}^{(0)}$ guaranteed by (4.7); the result is

$$(\nabla_\perp^2+2i\partial_T)\mathbf{a}_{\perp 1}^{(0)}=\bar{\eta}_0^{(0)}\mathbf{a}_{\perp 1}^{(0)} , \tag{4.9}$$

where $\bar{\eta}_0^{(0)}$ is the τ-averaged density. In Sec. IV A we will see that $\bar{\eta}_0^{(0)}$ is in fact the density calculated in the quasistatic approximation [9].

Using the conditions (4.3)–(4.7) in the slow equations (3.5)–(3.10) yield the lowest-order equations, which form the basis of our model:

$$\nabla\cdot\mathbf{a}_0^{(0)}=0 , \tag{4.10}$$

$$(\nabla_\perp^2+2\partial_\tau\partial_\xi-\partial_\tau^2)\mathbf{a}_0=\eta_0^{(0)}\mathbf{p}_0^{(0)}+\nabla(\partial_\tau-\partial_\xi)\phi_0^{(0)} , \tag{4.11}$$

$$\nabla^2\phi_0^{(0)}=\gamma_0^{(0)}\eta_0^{(0)}-n_i , \tag{4.12}$$

$$(\partial_\tau-\partial_\xi)(\mathbf{p}_0^{(0)}-\mathbf{a}_0^{(0)})=\nabla(\phi_0^{(0)}-\gamma_0^{(0)}) , \tag{4.13}$$

$$(\partial_\tau-\partial_\xi)(\eta_0^{(0)}\gamma_0^{(0)})+\nabla\cdot(\eta_0^{(0)}\mathbf{p}_0^{(0)})=0 . \tag{4.14}$$

We can relate the two-variable expansion presented above to the standard technique of matched asymptotic expansions ([20], Chap. 1) by noting that the derivatives with respect to the propagation variable T, in Eqs. (3.5)–(3.19), always occur in the combination $\theta\partial_T$. Differential equations in which the small parameter multiples the highest derivative terms typically display boundary layer behavior ([20], p. 345). In our case the situation is complicated by the appearance of negative powers of θ arising from the elimination of the optical scale oscillations. In order to meet this difficulty we will use a slight modification of the usual argument employed in the method of matched asymptotic expansions. The idea is to study the behavior of the solution in the limit $\theta\rightarrow 0$. We first examine the equations by expanding the solution in powers of θ in the "outer" region, where T is bounded away from the origin and the T derivatives are finite. Eliminating the negative powers of θ imposes the conditions (4.3)–(4.6) on the leading terms in the expansion. With these conditions in force, the fast equations (3.13)–(3.19) reduce to the paraxial wave equation:

$$(\nabla_\perp^2+2i\partial_T)\mathbf{a}_{\perp 1}^{(0)}=\eta_0^{(0)}\mathbf{a}_{\perp 1}^{(0)} , \tag{4.15}$$

and all T-derivative terms are eliminated from the slow equations (3.5)–(3.10). This is equivalent to setting all the T derivatives to zero in (3.5)–(3.10), and the resulting equations constitute the well-known quasistatic approximation [9]. In this limit the fluid variables follow the field adiabatically; therefore it is not possible to impose independent initial conditions on them. This circumstance is not surprising since the order of the fluid equations is reduced by setting $\theta=0$, but it does require further analysis in order to recover the freedom to impose initial data. For this purpose it is necessary to consider the solution in an infinitesimal $[O(\theta)]$ neighborhood of the origin. This is the "inner" region defined by finite values of the variable $\tau=T/\theta$. The inner expansion is obtained by setting $\partial_T=\partial_\tau/\theta$ and expanding in powers of θ. Elimination of the negative powers of θ, again yields (4.3)–(4.6), and in addition (4.7). In this limit $\theta\partial_T\to\partial_\tau$ so the order of the fluid equations remains unchanged, and arbitrary initial conditions can be accommodated. The inner and outer expansions determined in this way must be matched at some intermediate time in order to get a uniformly valid solution. The intermediate matching region constitutes the boundary layer, or in the present case initial layer. The dimensionless thickness, L_i, of the initial layer is order unity. In physical terms this means that L_i is large compared to the optical wavelength and small compared to the Rayleigh range $(1/k \ll L_i \ll L_R)$.

The two-variable expansion provides an alternative to the explicit matching procedure. Thus the outer expansion can be recovered by combining (4.8) with (4.10)–(4.14), imposing $\tau=T/\theta$ $(\partial_\tau=\theta\partial_T)$, and letting $\theta\to 0$. The result constitutes the QSA for the fluid equations:

$$\nabla\cdot\mathbf{a}_0^{(0)}=0 , \tag{4.16}$$

$$\nabla_\perp^2\mathbf{a}_0=\eta_0^{(0)}\mathbf{p}_0^{(0)}-\nabla\partial_\xi\phi_0^{(0)} , \tag{4.17}$$

$$\nabla^2\phi_0^{(0)}=\gamma_0^{(0)}\eta_0^{(0)}-n_i , \tag{4.18}$$

$$-\partial_\xi(\mathbf{p}_0^{(0)}-\mathbf{a}_0^{(0)})=\nabla(\phi_0^{(0)}-\gamma_0^{(0)}) , \tag{4.19}$$

$$-\partial_\xi(\eta_0^{(0)}\gamma_0^{(0)})+\nabla\cdot(\eta_0^{(0)}\mathbf{p}_0^{(0)})=0 . \tag{4.20}$$

Thus the QSA describes the asymptotic behavior of the solution after the transient oscillations in the initial layer have died out.

The inner expansion results from setting $T=\theta\tau(\partial_T=\partial_\tau/\theta)$, and taking the limit $\theta\to 0$. When (4.7) is used the result is simply to set the T derivative in (4.8) to zero. In this case Eqs. (4.10)–(4.14) are unchanged and (4.8) becomes

$$2i\partial_\tau\mathbf{a}_{\perp 1}^{(1)}=\eta_0^{(0)}\mathbf{a}_{\perp 1}^{(0)}-\nabla_\perp^2\mathbf{a}_{\perp 1}^{(0)} . \tag{4.21}$$

The integration of (4.21) will in general lead to unacceptable (secular) terms proportional to τ, since (4.6) shows that $\mathbf{a}_{\perp 1}^{(0)}$ is independent of τ. To avoid this difficulty, let us return to (4.8), and set $\eta_0^{(0)}=\bar\eta_0^{(0)}+\tilde\eta_0^{(0)}$, where $\bar\eta_0^{(0)}$ satisfies the asymptotic (quasistatic) equations (4.15)–(4.20). This means that $\tilde\eta_0^{(0)}$ will vanish at large τ. The secular terms can then be avoided by imposing

$$(\nabla_\perp^2+2i\partial_T)\mathbf{a}_{\perp 1}^{(0)}=\bar\eta_0^{(0)}\mathbf{a}_{\perp 1}^{(0)} , \tag{4.22}$$

$$2i\partial_\tau\mathbf{a}_{\perp 1}^{(1)}=\tilde\eta_0^{(0)}\mathbf{a}_{\perp 1}^{(0)} . \tag{4.23}$$

This eliminates the first-order term $\mathbf{a}_{\perp 1}^{(1)}$ from the zeroth-order problem, and identifies the long-time τ average with the QSA value.

V. THE FULLY RELATIVISTIC MODEL

We gather here the basic equations for the leading order of the uniform expansion, with the simplified notation $\mathbf{a}_{\perp 1}^{(0)}\to\mathbf{a}_L$ (leading-order laser amplitude), $\eta_0^{(0)}\to\eta$ (charge density in the local fluid rest frame), $\bar\eta_0^{(0)}\to\bar\eta$ (quasistatic charge density), $\mathbf{a}_0\to\mathbf{a}$ (vector potential due to wake motions), $p_0^{(0)}\to\mathbf{p}$ (electron momentum of wake motions), $\phi_0^0\to\phi$ (electrostatic potential), $\gamma_0^{(0)}\to\gamma$ (electron energy). At the same time we make use of (4.13) to introduce the potential Λ by

$$\mathbf{p}-\mathbf{a}=\nabla\Lambda . \tag{5.1}$$

This will allow the force equation (4.13) to be written in either of two forms. The resulting set of equations is

$$\partial_\tau\mathbf{a}_L=0 , \tag{5.2}$$

$$(\nabla_\perp^2+2i\partial_T)\mathbf{a}_L=\bar\eta\mathbf{a}_L , \tag{5.3}$$

$$\nabla\cdot\mathbf{a}=0 , \tag{5.4}$$

$$(\nabla_\perp^2+2\partial_\tau\partial_\xi-\partial_\tau^2)\mathbf{a}=\eta\mathbf{p}+\nabla(\partial_\tau-\partial_\xi)\phi , \tag{5.5}$$

$$\nabla^2\phi=\gamma\eta-n_i , \tag{5.6}$$

$$(\partial_\tau-\partial_\xi)\Lambda=\phi-\gamma , \tag{5.7}$$

$$(\partial_\tau-\partial_\xi)(\mathbf{p}-\mathbf{a})=\nabla(\phi-\gamma) , \tag{5.8}$$

$$(\partial_\tau-\partial_\xi)(\eta\gamma)+\nabla\cdot(\eta\mathbf{p})=0 , \tag{5.9}$$

$$\gamma=\sqrt{1+\mathbf{p}^2+(1/2)\mathbf{a}_L^*\cdot\mathbf{a}_L} . \tag{5.10}$$

The expression (5.10) for γ is obtained by combining (3.10), (4.5), and (4.4). The gauge condition (5.4) and the continuity equation (5.9) are not both required; each follows from the other with the aid of (5.5). The propagation equation (5.3) does not include dispersion. In the expansion used here dispersive terms would first appear in $O(\theta^2)$, so dispersive effects are small for sufficiently underdense plasmas.

A. The quasistatic approximation

As explained in Sec. IV, the solution of (5.2)–(5.10) asymptotically becomes independent of the plasma-scale variable τ. The asymptotic solution, denoted by $\bar\eta$, etc., will then obey the QSA equations [9]

$$(\nabla_\perp^2+2i\partial_T)\mathbf{a}_L=\bar\eta\mathbf{a}_L , \tag{5.11}$$

$$\nabla_\perp\cdot\bar{\mathbf{a}}_\perp+\partial_\xi\bar a_z=0 , \tag{5.12}$$

$$\nabla_\perp^2\bar{\mathbf{a}}_\perp=\eta\bar{\mathbf{p}}_\perp-\nabla_\perp\partial_\xi\bar\phi , \tag{5.13}$$

$$\nabla_\perp^2 \bar{a}_z = \bar{\eta}\bar{p}_z - \partial_\xi^2 \bar{\phi} \ , \tag{5.14}$$

$$\nabla_\perp^2 \bar{\phi} + \partial_\xi^2 \bar{\phi} = \bar{\gamma}\bar{\eta} - n_i \ , \tag{5.15}$$

$$\partial_\xi(\bar{\mathbf{p}} - \bar{\mathbf{a}}) = \nabla(\bar{\gamma} - \bar{\phi}) \ . \tag{5.16}$$

Following Sprangle *et al.* [9], we now show that the quasistatic equations can be reduced to a pair of equations for the laser field $\mathbf{a}_L$ and the wake potential $\psi = \phi - a_z$. Since the analysis is carried out entirely in the QSA, the notation $\bar{\eta}$, etc., will be dropped. We first observe that the z component of (5.16) implies that $(\gamma - \phi + a_z - p_z)$ is independent of ζ. Since this quantity has the value one for large positive ζ, i.e., before the arrival of the pulse, we have

$$p_z = \gamma - (\psi + 1) \ . \tag{5.17}$$

This result allows γ, given by (5.10), to be expressed as a function of $\mathbf{a}_L$, $\mathbf{p}_\perp$, and ψ:

$$\gamma = \frac{1 + \mathbf{p}_\perp^2 + (1/2)\mathbf{a}_L^* \cdot \mathbf{a}_L + (\psi+1)^2}{2(\psi+1)} \ . \tag{5.18}$$

The proper density η can be expressed as a function of ψ by eliminating $\partial_\xi^2 \phi$ between (5.14) and (5.15), and using (5.17) to get

$$\eta = \frac{n_i + \nabla_\perp^2 \psi}{1 + \psi} \ . \tag{5.19}$$

Under some conditions, e.g., when cavitation is possible, (5.19) may yield negative values for η. In this case the right-hand side of (5.19) should be replaced by zero [6]. To find the transverse electron momentum $\mathbf{p}_\perp$, substitute $\phi = \psi + a_z$ into (5.13) and use (5.12) to eliminate $\partial_\xi a_z$; the result is

$$\eta \mathbf{p}_\perp - \nabla_\perp \partial_\xi \psi = \nabla_\perp^2 \mathbf{a}_\perp - \nabla_\perp(\nabla_\perp \cdot \mathbf{a}_\perp) \ . \tag{5.20}$$

The curl of the transverse part of (5.16) gives $\partial_\xi[\nabla_\perp \times (\mathbf{p}_\perp - \mathbf{a}_\perp)] = 0$, which in turn implies $\nabla_\perp \times \mathbf{p}_\perp = \nabla_\perp \times \mathbf{a}_\perp$, since both $\mathbf{p}_\perp$ and $\mathbf{a}_\perp$ vanish at large positive ζ. This observation, together with the identity $\nabla_\perp \times (\nabla_\perp \times \mathbf{F}_\perp) = \nabla_\perp(\nabla_\perp \cdot \mathbf{F}_\perp) - \nabla_\perp^2 \mathbf{F}_\perp$ shows that $\nabla_\perp^2 \mathbf{a}_\perp - \nabla_\perp(\nabla_\perp \cdot \mathbf{a}_\perp) = \nabla_\perp^2 \mathbf{p}_\perp - \nabla_\perp(\nabla_\perp \cdot \mathbf{p}_\perp)$; therefore the transverse potential $\mathbf{a}_\perp$ can be eliminated from (5.20) which becomes

$$\nabla_\perp^2 \mathbf{p}_\perp - \nabla_\perp(\nabla_\perp \cdot \mathbf{p}_\perp) - \eta \mathbf{p}_\perp = -\nabla_\perp \partial_\xi \psi \ . \tag{5.21}$$

Thus $\mathbf{p}_\perp$ is determined in terms of ψ as the solution of a differential equation which only involves transverse derivatives. In the special case of cylindrical symmetry, the identity $\nabla_\perp^2 \mathbf{p}_\perp - \nabla_\perp(\nabla_\perp \cdot \mathbf{p}_\perp) = 0$ simplifies (5.21) to

$$\mathbf{p}_\perp = \frac{1}{\eta} \nabla_\perp \partial_\xi \psi \tag{5.22}$$

wherever $\eta \neq 0$. If cavitation occurs, i.e., $\eta \equiv 0$ in some region, then the cylindrically symmetric form of (5.21) simply shows that $\nabla_\perp \partial_\xi \psi = 0$, and provides no information about $\mathbf{p}_\perp$. This is of no consequence since the fluid velocity has no meaning in the absence of any electrons [6]. The remaining equation for ψ is obtained by taking the divergence of (5.16), and using (5.12), (5.14), and (5.17) to get [23],

$$\partial_\xi^2 \psi = \gamma\eta - n_i - \nabla_\perp^2 \gamma + \partial_\xi \nabla_\perp \cdot \mathbf{p}_\perp \ . \tag{5.23}$$

The QSA is thus reduced to a pair of propagation equations, (5.11) and (5.23), for $\mathbf{a}_L$ and ψ respectively, together with the subsidiary equations (5.18), (5.19), and (5.21) [or (5.22)], which define the variables γ, η, and $\mathbf{p}_\perp$ as functions of ψ and $\mathbf{a}_L$. The vector potential $\mathbf{a}$ can then be calculated by integrating the transverse part of (5.16) together with the divergence condition (5.12).

B. Plane-wave stability of the QSA

For a spatially uniform plasma, i.e., for $n_i(\mathbf{r}) \equiv 1$, the QSA has an exact plane wave solution given by

$$\mathbf{a}_{L0} = \mathbf{u} A_0 e^{-i\Omega_0 T} \ , \quad \Omega_0 = \frac{\eta_0}{2} \ , \quad \gamma_0 = \sqrt{1 + A_0^2/2} \ ,$$
$$\eta_0 \gamma_0 = 1 \ , \quad \psi_0 = \gamma_0 - 1 \ , \quad \mathbf{p}_{\perp 0} = \mathbf{0} \ . \tag{5.24}$$

We now consider a perturbation to this solution of the form

$$\mathbf{a}_L \to \mathbf{a}_{L0} + \delta\mathbf{a}_L = \mathbf{u}(A_0 + \delta A) e^{-i\Omega_0 T} \ ,$$
$$\psi \to \psi_0 + \delta\psi \ , \tag{5.25}$$

and further write the complex function δA in terms of its real and imaginary parts, $\delta A = \delta U + i\delta V$. The first-order corrections for γ, η, and $\mathbf{p}_\perp$ are computed from (5.18), (5.19), and (5.21). Linearizing Eqs. (5.11) and (5.23) in this way yields

$$2\partial_T \delta U = -\nabla_\perp^2 \delta V \ , \tag{5.26}$$

$$2\partial_T \delta V = \nabla_\perp^2 \delta U + \frac{A_0}{\gamma_0^2}(1 - \gamma_0 \nabla_\perp^2)\delta\psi \ , \tag{5.27}$$

$$(1 + \gamma_0 \partial_\xi^2)\delta\psi = \frac{A_0}{2\gamma_0} \delta U \ . \tag{5.28}$$

Fourier transforming these equations with respect to $\mathbf{r}_\perp$, ζ, and T produces the dispersion relation

$$\Omega^2 = \frac{q_\perp^2}{2}\left[\frac{q_\perp^2}{2} + \frac{A_0^2(1 + \gamma_0 q_\perp^2)}{4\gamma_0^3(\gamma_0 q_\xi^2 - 1)}\right] \ , \tag{5.29}$$

where $\mathbf{q}_\perp$, q_ξ, and Ω are, respectively, conjugate to $\mathbf{r}_\perp$, ζ, and T.

For $\gamma_0 q_\xi^2 < 1$ the QSA dispersion relation (5.29) predicts growth rates that increase without bound as $|\mathbf{q}_\perp| \to \infty$. Similar results were obtained by Antonsen and Mora [24] in the weak-relativity limit. Since q_ξ is measured in units of the plasma wave number, k_P, this means that perturbations with wave numbers less than $k_P/\sqrt{\gamma_0}$ will be unstable. Indeed when the dimensionless wave number q_ξ satisfies $0 < (1 - \gamma_0 q_\xi^2) < A_0^2/(2\gamma_0^2)$, the perturbation is unstable for all values of $\mathbf{q}_\perp$, and for large $|\mathbf{q}_\perp|$ the growth rate increases as $q_\perp^4$. Thus for longitudinal momenta sufficiently close to the critical value $k_p/\sqrt{\gamma_0}$, the plane-wave solution (5.24) is unstable to perturbations

on arbitrarily small transverse distance scales. The divergence of the growth rate as $|\mathbf{q}_\perp| \to \infty$ is an artifact of the QSA and will be removed when a more accurate dispersion relation is used [25]. In addition, the finite duration of a realistic pulse will tend to suppress the instability by imposing a bound on the growth rates of small-scale transverse perturbations. This effect will be most pronounced for short pulses, but longer pulses more closely resembling plane waves can be expected to show significant pulse modulation. The existence of these modulations can cause numerical instabilities that make the use of the QSA for such simulations questionable. In the context of the weak-field limit considered in the next section, we will show how to improve the QSA so that these instability problems can be reduced.

Another shortcoming of (5.29) is that it does not describe forward Raman scattering [26]. This follows from the observation that $\Omega=0$ when $q_\perp=0$. This defect can be repaired by including the leading dispersive term in the propagation equation (5.3) [27]. This yields the modified dispersion relation

$$\Omega^2=\frac{q_\perp^2+\theta^2 q_\xi^2}{2}\left[\frac{q_\perp^2+\theta^2 q_\xi^2}{2}+\frac{A_0^2(1+\gamma_0 q_\perp^2)}{4\gamma_0^3(\gamma_0 q_\xi^2-1)}\right] . \tag{5.30}$$

The θ^2 terms are only significant for very small $q_\perp$. For a beam with finite spot size w, $(q_\perp)_{\rm rms}\approx 1/w$ so dispersion will be unimportant for spot sizes satisfying $k_p w \ll 1/\theta^2$ (conventional units). This condition is well satisfied in high-intensity experiments where the incident laser beams are tightly focused. The subsequent self-focusing of the beam renders dispersive effects even less important.

VI. THE WEAK-FIELD LIMIT

As a first application of the model described above, we will consider weak fields with $|\mathbf{a}_L|<1$. For example, assuming 1-μm radiation, the value $|\mathbf{a}_L|\approx 0.3$ corresponds to an intensity $I\approx 10^{17}$ W/cm^2 and a quiver velocity $v/c\approx 0.3$. The full equations (5.2)–(5.10) can then be approximated by keeping only the leading relativistic corrections. This approximation has been previously discussed by several authors [24,28–30].

Since the laser amplitude $\mathbf{a}_L$ enters into the fluid equations only through the term $|\mathbf{a}_L|^2$ in (5.10), the fluid quantities $\mathbf{p}$, $\mathbf{a}$, and n, where

$$n\equiv\gamma\eta-n_i , \tag{6.1}$$

are all first order in $|\mathbf{a}_L|^2$. Thus the $\mathbf{p}^2$ term in (5.10) is second order and

$$\gamma=1+\tfrac{1}{4}|\mathbf{a}_L|^2+O(|\mathbf{a}_L|^4) . \tag{6.2}$$

The expansion for η is obtained by inverting the definition (6.1) of n:

$$\eta=n_i+n-\tfrac{1}{4}n_i|\mathbf{a}_L|^2+\cdots . \tag{6.3}$$

The weak-field equations are obtained by inserting these expansions into (5.2)–(5.7)

$$\partial_\tau \mathbf{a}_L=0 , \tag{6.4}$$

$$(\nabla_\perp^2+2i\partial_T)\mathbf{a}_L=\{\bar{n}_i+\bar{n}-\tfrac{1}{4}\bar{n}_i|\mathbf{a}_L|^2\}\mathbf{a}_L , \tag{6.5}$$

$$\nabla\cdot\mathbf{a}=0 , \tag{6.6}$$

$$(\nabla_\perp^2+2\partial_\tau\partial_\xi-\partial_\tau^2)\mathbf{a}=n_i\mathbf{a}+n_i\nabla\Lambda+\nabla(\partial_\tau-\partial_\xi)\phi , \tag{6.7}$$

$$\nabla^2\phi=n , \tag{6.8}$$

$$(\partial_\tau-\partial_\xi)\Lambda=\phi-\tfrac{1}{4}|\mathbf{a}_L|^2 . \tag{6.9}$$

In certain special situations the wake vector potential $\mathbf{a}$ vanishes identically. The necessary conditions are obtained by applying the curl operation to (6.7), and setting $\mathbf{a}=0$ to get

$$\nabla n_i\times\nabla\Lambda=0 . \tag{6.10}$$

This condition is satisfied for a homogeneous plasma ($n_i\equiv 1$), and it is also satisfied in planar geometries for which n_i and Λ only depend on z. The latter alternative will be considered in Sec. VI A, but for the remainder of this section, we will assume that the plasma is initially homogeneous.

For the case $n_i\equiv 1$, the divergence of (6.7) combined with (6.8) produces

$$\nabla^2\Lambda+\nabla^2(\partial_\tau-\partial_\xi)\phi=0\Longrightarrow\nabla^2\Lambda=-(\partial_\tau-\partial_\xi)n , \tag{6.11}$$

and this, combined with the action of $\partial_t=(\partial_t-\partial_\xi)$ on (6.9), finally gives

$$[(\partial_\tau-\partial_\xi)^2+1]n=\tfrac{1}{4}\nabla^2|\mathbf{a}_L|^2 . \tag{6.12}$$

Similar manipulations lead to equations for the potentials ϕ and Λ:

$$[(\partial_\tau-\partial_\xi)^2+1]\phi=\tfrac{1}{4}|\mathbf{a}_L|^2 , \tag{6.13}$$

$$[(\partial_\tau-\partial_\xi)^2+1]\Lambda=\tfrac{1}{4}\partial_\xi|\mathbf{a}_L|^2 . \tag{6.14}$$

The weak-field model is completely specified by (6.4), (6.5), and (6.12). Since (6.4) guarantees that the right-hand side of (6.12) is independent of τ, the general solution of (6.12) can be expressed as the sum of a special solution independent of τ, and the general solution of the homogeneous equation, i.e.,

$$n(\mathbf{r}_\perp,\xi,T,\tau)=\bar{n}(\mathbf{r}_\perp,\xi,T)+\tilde{n}(\mathbf{r}_\perp,\xi,T,\tau) , \tag{6.15}$$

where $\bar{n}(\mathbf{r}_\perp,\xi,T)$ and $\tilde{n}(\mathbf{r}_\perp,\xi,T,\tau)$ satisfy

$$[\partial_\xi^2+1]\bar{n}=\tfrac{1}{4}\nabla^2|\mathbf{a}_L|^2 , \tag{6.16}$$

$$[(\partial_\tau-\partial_\xi)^2+1]\tilde{n}=0 . \tag{6.17}$$

In this simple model the propagation equation (6.5) and the quasistatic equation (6.16) formally decouple from the equation for $\tilde{n}$, the τ-dependent part of the density, but the solution of (6.17) must be chosen so that the total density $n=\bar{n}+\tilde{n}$ satisfies the initial conditions at $T=\theta\tau=0$.

A. Exact 1D solutions

Useful insights into the weak field limit can be obtained by considering a simpler problem in which the undisturbed plasma and the incident laser pulse are planar, i.e.,

independent of the transverse coordinates. Then there are 1D solutions obtained by neglecting the transverse dependence of all the variables. This simplification allows us to examine explicitly features of the general solution, such as the transient behavior in the initial layer. It is also important to point out that the same results can be obtained for averages of the intensity and density over the transverse coordinates, with no assumptions made about the transverse profile of the input pulse. This can be seen by integrating the fluid equations over the transverse coordinates and using the conservation of the total power passing through a given ζ plane. This results in equations of the same form as those given below for the 1D case.

The condition (6.10), which implies $\mathbf{a}=0$, is automatically satisfied for planar geometries, even if the plasma is longitudinally inhomogeneous. In order to allow for this possibility, it is convenient to replace the potentials ϕ and Λ by the longitudinal fluid momentum, $p=\partial_\zeta\Lambda$, and the longitudinal electric field, $\varepsilon=-\partial_\zeta\phi$. The dynamical equations for p, n, and ε are easily derived from (6.7)–(6.9). The final simplification for this case is the assumption that the inhomogeneous ion density is stationary, i.e., $n_i=n_i(z)$, or $\partial_t n_i=(\partial_\tau-\partial_\zeta)n_i=0$. With this fact in mind, manipulations similar to those used in the homogeneous case lead to

$$2i\partial_T\mathbf{a}_L=\{\bar{n}_i+\bar{n}-\tfrac{1}{4}\bar{n}_i|\mathbf{a}_L|^2\}\mathbf{a}_L\ , \tag{6.18}$$

$$[(\partial_\tau-\partial_\zeta)^2+n_i]\varepsilon=-\tfrac{1}{4}n_i\partial_\zeta|\mathbf{a}_L|^2\ , \tag{6.19}$$

$$[(\partial_\tau-\partial_\zeta)^2+n_i]p=\tfrac{1}{4}\partial_\zeta^2|\mathbf{a}_L|^2\ . \tag{6.20}$$

$$n=-\partial_\zeta\varepsilon\ . \tag{6.21}$$

Since $n_i=n_i(z)=n_i(\zeta+\tau)$, the τ-asymptotic form $\bar{n}_i$ represents the ion density deep in the plasma. We will assume that the plasma density is uniform in this region so that $\bar{n}_i$ is a constant. Inspection of (6.18) shows that $\partial_T|\mathbf{a}_L|^2=0$; so the right-hand side of (6.19) is independent of T as well as τ. The QSA electric field $\bar{\varepsilon}$ satisfies

$$[\partial_\zeta^2+n_i]\bar{\varepsilon}=-\tfrac{1}{4}\bar{n}_i\partial_\zeta|\mathbf{a}_L|^2\ , \tag{6.22}$$

with the same right-hand side, therefore it is also independent of T. The asymptotic limit of (6.21) yields

$$\bar{n}=-\partial_\zeta\bar{\varepsilon}\ , \tag{6.23}$$

which shows that the QSA density $\bar{n}$ is also independent of T. Therefore (6.18) has the solution

$$\mathbf{a}_L(\zeta,T)=\exp\left[-\frac{i}{2}[\bar{n}_i+\bar{n}(\zeta)-\tfrac{1}{4}\bar{n}_i I_L(\zeta)]T\right]\mathbf{a}_L(\zeta,0)\ , \tag{6.24}$$

where $I_L(\zeta)\equiv|\mathbf{a}_L(\zeta,0)|^2$. This exhibits self-phase modulation of the laser pulse. The fluid equations (6.19) and (6.20) can be solved by reverting to laboratory coordinates, i.e., $(\partial_\tau-\partial_\zeta)\to\partial_t$, and making the change of variables $u=\Omega(z)t$, with $\Omega(z)\equiv\sqrt{n_i(z)}$. This yields an ordinary differential equation that can be solved by variation of constants. With the initial conditions $\varepsilon(z,0)=\partial_t\varepsilon(z,0)=0$, the electric field is given by

$$\varepsilon(\zeta,\tau)=-\tfrac{1}{4}\Omega(\zeta+\tau)\int_0^\tau d\tau'\,\partial_\zeta I_L(\zeta+\tau')\times\sin[\Omega(\zeta+\tau)\tau']\ . \tag{6.25}$$

As $\tau\to\infty$, (6.25) shows that $\varepsilon(\zeta,\tau)\to\bar{\varepsilon}(\zeta)$, which is a solution of (6.21). Similar results can be obtained for $p(\zeta,\tau)$ and $n(\zeta,\tau)$.

Study of the transient phenomena expected to occur in the initial layer requires a careful consideration of the initial conditions for the physical problem [27]. For this purpose it is useful to replace the familiar Gaussian pulse by a pulse with *finite support*, i.e., a smooth pulse that vanishes outside some finite interval on the ζ axis. Let the plasma occupy the region $z>0$, and suppose that $I_L(\zeta)$ vanishes identically for all $\zeta>0$. Physically this means that the leading edge of the pulse reaches the plasma at $t=0$. In the region occupied by the plasma, $\zeta+\tau>0$, (6.25) becomes

$$\varepsilon(\zeta,\tau)=-\tfrac{1}{4}\Omega(\zeta+\tau)\int_0^{-\zeta}d\tau'\partial_\zeta I_L(\zeta+\tau')\times\sin[\Omega(\zeta+\tau)\tau']\ , \tag{6.26}$$

so the τ dependence comes entirely from $\Omega(\zeta+\tau)=\sqrt{n_i(\zeta+\tau)}$, in other words from the longitudinal inhomogeneity of the ion density. In particular if the ion density is homogeneous, then (6.26) has no τ dependence at all, and it is easy to show that it satisfies (6.22). Thus the QSA solution is in fact the exact solution for a finite pulse entering a longitudinally homogeneous plasma.

A simple approximation to a finite pulse, peaked at $\zeta=\zeta_0$, is given by

$$I_L(\zeta)=A_0^2\theta(2\sqrt{\ln 2}L_p-|\zeta-\zeta_0|)\times\cos^2\left[\frac{\pi(\zeta-\zeta_0)}{4\sqrt{\ln 2}L_p}\right]\ , \tag{6.27}$$

where $\theta(x)$ is the usual step function. The normalization of L_p has been chosen so that the finite pulse has the same full width at half maximum (FWHM) as the Gaussian pulse $\exp(-\zeta^2/L_p^2)$. With this form for the pulse the integral (6.25) can be carried out explicitly, and used to produce the numerical examples presented below.

Denote the pulse duration in conventional units by T_p^*, then

$$T_p^*=0.56L_p/\theta\,\text{fs}=0.56L_p\sqrt{N_c/N_e}\,\text{fs}\ . \tag{6.28}$$

The current limitations of laser technology make it difficult to achieve high-energy pulses with durations much shorter than 100 fs. For this reason, we will make our numerical estimates using the practical lower limit $T_p^*>100$ fs for the pulse duration. Combining this restriction with (6.28) imposes a relation between the dimensionless pulse length and the small parameter θ:

$$L_p=1.79\theta T_p^*[\text{fs}]>179\theta=179\sqrt{N_e/N_c}\ . \tag{6.29}$$

In all the examples discussed in this section we choose the initial time, $t=0$, as the arrival time of the leading edge of the pulse at the beginning of the plasma region;

this corresponds to the choice $\zeta_0=-2\sqrt{\ln 2}L_p$. We also assume that the ion density ramps up from the vacuum over a distance σ, according to the model $n_i(z)=\theta(z)\{\theta(\sigma-z)\sin^2(\pi z/2\sigma)+\theta(z-\sigma)\}$, which is continuous and has a continuous first derivative everywhere. For a nominal plasma wavelength $\lambda=1$ μm, and $\theta=0.015$ ($N_e/N_c=2.25\times10^{-4}$), a typical ramp length of 2 mm corresponds to $\sigma=180$; this value is used in all examples.

The short-pulse limit is particularly relevant to the study of laser accelerations [31,32]. Indeed, the optimum pulse length for the standard laser wake-field acceleration scheme is $L_p=\pi$, or in conventional units, $L_p=\lambda_P/2$ [5]. According to (6.29) $L_p=\pi$ is only feasible for $\theta<0.0175$ ($N_e/N_c<3.1\times10^{-4}$). For this application the most interesting quantity is the longitudinal electric (wake) field. In the wake region ($\zeta-\zeta_0<-2\sqrt{\ln 2}L_p$) the QSA electric field oscillates with period λ_P and has a peak amplitude 496 MV/m. The transient behavior of the full solution is shown in Fig. 1, where we plot the transient field at $\zeta=-2\pi$ (the location of a QSA peak) as a function of τ. Since the pulse length is small compared to the ramp length ($L_p\ll\sigma$), the entire pulse propagates through the ramp in the transit time $\Delta\tau_{\text{ramp}}\approx\sigma\approx180$. The peak transient field is comparable to the peak QSA field, and the transient solution decays to the QSA value after the time $\tau_{\text{decay}}\approx\Delta\tau_{\text{ramp}}$. Another way of comparing the transient and QSA fields is to plot both as functions of ζ for a fixed value of τ. In Fig. 2, we choose $\tau=67.9$, which corresponds to the peak of the transient field in Fig. 1.

The QSA peak fields are sensitive to departures from the optimum value $L_p=\lambda_P/2$; for example, if $L_p=\lambda_P$, the peak value is reduced to 80 MV/m. By contrast, the transient field is much less sensitive, as shown in Fig. 3, where the peak value is larger than that seen in Fig. 1. Again the transient solution approaches the QSA limit after about one transit time across the density ramp. The ζ dependence of the transient field is shown in Fig. 4 for $\tau=67.6$, corresponding to the peak in Fig. 3. At this early time the ζ profile of the transient field differs very significantly from that of the QSA field.

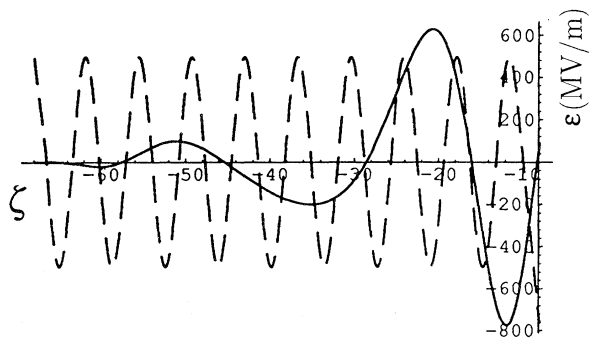

FIG. 2. $\varepsilon(\zeta,\tau)$ at $\tau=67.9$ ($t\approx2.5$ ps) (solid curve) and $\bar{\varepsilon}(\zeta)$ (dashed curve) vs ζ. Other parameters as in Fig. 1.

Long pulses are not suited to wake-field acceleration schemes, but they are important for channeling experiments. In this limit it is accordingly more useful to display the charge density rather than the field. For $L_p=60$ (approximately ten plasma wavelengths) (6.29) implies $n_e/n_c<0.11$. We plot in Fig. 5 the transient density at the pulse peak. The decay time for the plasma oscillations is given by $\tau_{\text{decay}}\approx\Delta\tau_{\text{ramp}}+L_p=240$. In this case the QSA value, $\bar{n}\approx2\times10^{-5}$, is two orders of magnitude smaller than the transient peak value. In Fig. 6 we plot the transient density for $\tau=111$, the location of one of the peaks in Fig. 5. The transient density profile shows the expected dip at the pulse maximum.

The 1D results presented above are equally valid for the transversely averaged density and intensity. Thus as far as these averaged quantities are concerned, the 1D results can be used without any assumption about the transverse profile of the incident laser pulse. This fact can provide useful insight into the behavior of the solution for the general case of nonplanar pulses, but some care is needed in interpreting the results. In particular

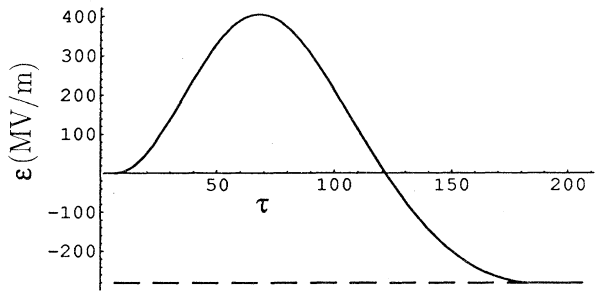

FIG. 1. Transient longitudinal electric field $\varepsilon(\zeta,\tau)$ (in MV/m) (solid) and QSA field $\bar{\varepsilon}(\zeta)$ (dashed) vs τ, at $\zeta=-2\pi$ for $L_p=\pi$. Assuming $\lambda=1$ μm, $\theta=0.015$, and $A_0=0.3$, this corresponds to $Z=-66.67$ μm and $T_p^*=117$ fs.

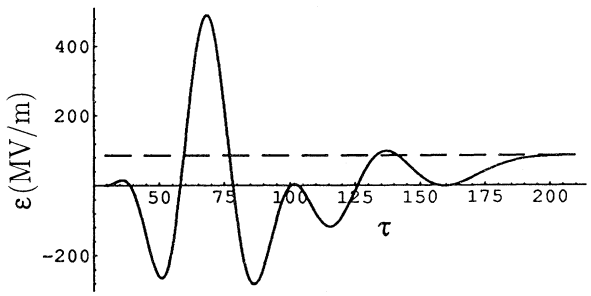

FIG. 3. $\varepsilon(\zeta,\tau)$ vs τ at $\zeta=-29.4$ ($Z=-0.33$ mm) for $L_p=\lambda_p$ ($T_p^*=234$ fs). Other parameters as in Fig. 1.

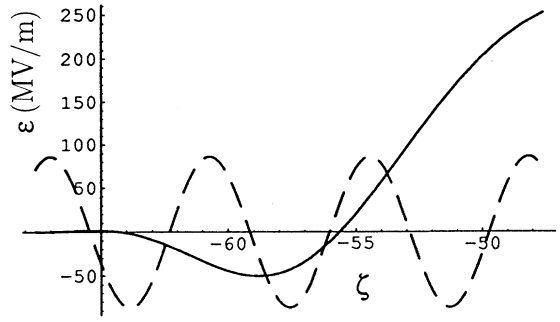

FIG. 4. $\varepsilon(\zeta,\tau)$ vs ζ at $\tau=67.6$ ($t\approx 2.5$ ps). Same parameters as Fig. 3.

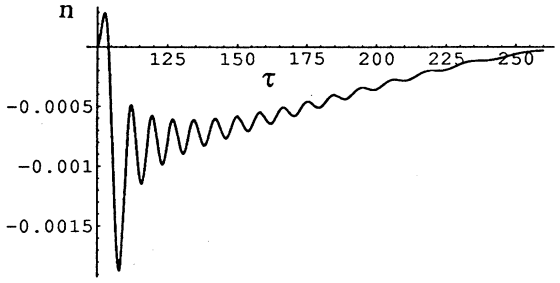

FIG. 5. Deviation from background density $n(\zeta,\tau)$ vs τ at the pulse peak, $\zeta=-99.9$, ($Z=-1.1$ mm) for $L_p=60$ ($T_p^*=2.2$ ps).

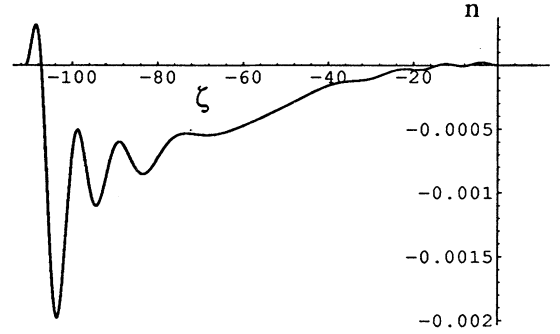

FIG. 6. $n(\zeta,\tau)$ vs ζ at $\tau=111$ ($t=4.1$ ps) for $L_p=60$ ($T_p^*=2.2$ ps).

the solutions presented here are formally valid for any pulse duration, no matter how large. Since the initial layer thickness is several times the pulse duration, this implies that the initial layer can be any size. For moderate pulse durations, i.e., $k_pL_p \ll 1/\theta$, the initial layer thickness for the planar solution agrees with the general scaling argument presented in Sec. IV, but for long pulses, $k_pL_p \geq 1/\theta$, the planar result gives a much larger initial layer. This means that the planar result, although exact, is not very useful for describing the propagation of a transverse modulation. For this purpose, true 3D calculations are required. In the following section we begin the study of transverse effects by considering the stability of plane-wave solutions with respect to transverse modulations.

B. An improved quasistatic approximation

The weak-field equations (6.4), (6.5), and (6.12) have a plane-wave solution

$$\mathbf{a}_{L0}=\mathbf{u}A_0e^{-i\Omega_0 T},\quad \Omega_0=\tfrac{1}{2}(1-\tfrac{1}{4}A_0^2),\quad n_0=0\ . \tag{6.30}$$

Assuming a perturbed solution of the form $a_L=(A_0+\delta A)e^{-i\Omega_0 T}$, $n=\delta n$ and linearizing yields

$$\partial_\tau \delta a_L=0\ , \tag{6.31}$$

$$(\nabla_\perp^2+2i\partial_T)\delta A=A_0\{\overline{\delta n}-\tfrac{1}{2}A_0\mathrm{Re}(\delta A)\}\ , \tag{6.32}$$

$$[(\partial_\tau-\partial_\zeta)^2+1]\delta n=\frac{A_0}{2}\nabla^2\mathrm{Re}(\delta A)\ . \tag{6.33}$$

Since these linear equations have the same structure as the 1D equations studied in Sec. VI A, the solutions can be obtained in the same way, and a Fourier transform yields the weak-field limit of the dispersion relation (5.29):

$$\Omega^2=\frac{q_\perp^2}{2}\left[\frac{q_\perp^2}{2}+\frac{A_0^2(1+q_\perp^2)}{4(q_\zeta^2-1)}\right]\ . \tag{6.34}$$

This result shows that, while the two-variable expansion scheme does correctly deal with the transient behavior in the initial layer, it does not escape the instabilities associated with the (τ asymptotic) QSA. In previous numerical simulations the QSA instabilities have been treated by *ad hoc* filtering methods [24], but these techniques do not arise naturally from the mathematical problem at hand. On the other hand, the inner and outer solutions discussed in Sec. IV do provide a natural method for softening the singularities. In the outer form of the weak-field equations, (6.4) would not appear and the τ derivatives in (6.12) would be replaced by $\partial_\tau\rightarrow\theta\partial_T$. The linearized perturbation equations (6.31)–(6.33) would then be replaced by

$$(\nabla_\perp^2+2i\partial_T)\delta A=A_0\{\delta n-\tfrac{1}{2}A_0\mathrm{Re}(\delta A)\}\ , \tag{6.35}$$

$$[(\theta\partial_T-\partial_\zeta)^2+1]\delta n=\frac{A_0}{2}\nabla^2\mathrm{Re}(\delta A)\ , \tag{6.36}$$

corresponding to the dispersion relation, see also [24,25],

$$\Omega^2=\frac{q_\perp^2}{2}\left[\frac{q_\perp^2}{2}+\frac{A_0^2}{4}\frac{1+q_\perp^2+2\theta q_\zeta\Omega-\theta^2\Omega^2}{(q_\zeta-\theta\Omega)^2-1}\right], \tag{6.37}$$

which reduces to (6.34) for $\theta=0$. The most serious instability in the QSA occurs at $q_\zeta=1$, where (6.34) has a pole. In the vicinity of the pole, it is reasonable to neglect the entire θ dependence in the numerator and to retain only the leading $[O(\theta)]$ term in the denominator of (6.37). This leads to the approximate dispersion relation

$$\Omega^2=\frac{q_\perp^2}{2}\left[\frac{q_\perp^2}{2}+\frac{A_0^2}{4}\frac{1+q_\perp^2}{q_\zeta^2-1-2q_\zeta\theta\Omega}\right]. \tag{6.38}$$

For the critical mode $q_\zeta=1$, this cubic equation has no complex roots outside the region $q_\perp<q_{\perp c}$, where

$$\frac{q_{\perp c}^4}{1+q_{\perp c}^2}=1.3\frac{A_0^2}{\theta}. \tag{6.39}$$

This means that there are no unstable modes for transverse length scales smaller than $1/q_{\perp c}$. The same analysis shows that the growth rate $\Gamma=|\mathrm{Im}\Omega|$ is bounded by $A_0/\sqrt{\theta}$ when $A_0^2\ll\theta$ and by A_0^2/θ when $A_0^2\gg\theta$. Therefore the modified dispersion relation (6.38) eliminates the unbounded growth rates of the QSA. Similar results hold for the real part of the complex frequency, so $\theta\Omega$ satisfies either $|\theta\Omega|<\sqrt{\theta}A_0$ or $|\theta\Omega|<A_0^2$. This justifies the approximations used in obtaining (6.38) from (6.37), since the assumptions $A_0\ll1$ and $\theta\ll1$ guarantee $|\theta\Omega|\ll1$.

The improved stability resulting from the approximate dispersion relation (6.38) suggests the following modification for the numerical simulation of the weak field model. First recall that the version of (6.12) appropriate to the outer expansion is

$$[\partial_\zeta^2-2\theta\partial_\zeta\partial_T+\theta^2\partial_T^2+1]n=\tfrac{1}{4}\nabla^2|\mathbf{a}_L|^2. \tag{6.40}$$

Now consider a difference scheme for (6.5) with step size ΔT. In the step $T_j\to T_{j+1}=T_j+\Delta T$, we replace the quasistatic equation (6.16) by

$$[\partial_\zeta^2-2\theta\partial_\zeta\partial_T+1]\bar{n}=\tfrac{1}{4}\nabla^2|\mathbf{a}_L|^2, \tag{6.41}$$

where the $O(\theta^2)$ term in (6.40) has been dropped, in line with the approximations leading to (6.38), and the right-hand side, evaluated at $T=T_j$, is independent of T. Thus instead of allowing the quasistatic part of the density to follow the field adiabatically, we determine the density at T_{j+1} by integrating (6.41). The improved stability associated with the dispersion relation (6.38) suggests that this procedure will suppress the most damaging QSA instability. The modified QSA equation (6.41) has been previously considered by Mori *et al.* [26] in connection with forward Raman scattering.

C. Variational formulation of the improved QSA

It is known that the combination of Maxwell's equations with the relativistic fluid equations is a Hamiltonian system [19], and the QSA equations [(5.11)–(5.16)] have also been derived from a variational principle by averaging the exact Lagrangian over the rapid pulse oscillations [12]. It is therefore natural to expect that the improved QSA equations (6.5) and (6.41) can also be derived from a variational principle. For this purpose, the electrostatic potential is a more convenient variable than the charge density. The improved QSA equation for ϕ is

$$[\partial_\zeta^2-2\theta\partial_\zeta\partial_T+1]\bar{\phi}=\tfrac{1}{4}|\mathbf{a}_L|^2. \tag{6.42}$$

This follows from (6.13) by means of the substitution $\partial_\tau\to\theta\partial_T$ and the subsequent neglect of the $O(\theta^2)$ term. The improved QSA defined by (6.42) and (6.5) can be derived from the variational principle

$$\delta\int dt\int d\zeta\int d^2r_\perp\{\mathcal{L}_a+\mathcal{L}_\phi+\mathcal{L}_{\mathrm{int}}\}=0, \tag{6.43}$$

$$\mathcal{L}_a=i(a_L^*\partial_T a_L-\mathrm{c.c.})-|\nabla_\perp a_L|^2-n_i|a_L|^2+\frac{n_i}{8}|a_L|^4, \tag{6.44}$$

$$\mathcal{L}_\phi=4(\partial_\zeta\nabla^2\phi)(\theta\partial_T\phi)+2(\partial_\zeta\nabla\phi)\cdot(\partial_\zeta\nabla\phi)-2\nabla\phi\cdot\nabla\phi, \tag{6.45}$$

$$\mathcal{L}_{\mathrm{int}}=-|a_L|^2\nabla^2\phi. \tag{6.46}$$

The Hamiltonian corresponding to (6.43) is

$$H=\int d\zeta\int d^2r_\perp\left\{|\nabla_\perp a_L|^2-n_i\left[1-\frac{|a_L|^2}{8}\right]|a_L|^2+2(\nabla\phi)^2-2(\nabla\partial_\zeta\phi)^2+|a_L|^2\nabla^2\phi\right\}. \tag{6.47}$$

Since the Hamiltonian H is a constant of the motion, its numerical value is determined by the initial conditions. This fact constrains the later behavior of the solution, especially with regard to possible singularities. In addition H satisfies a minimum principle, so it can be used as the basis for approximate variational calculations.

VII. SIMULATION RESULTS IN THE WEAK-FIELD LIMIT

We describe here simulations of the weak-field model defined by (6.4), (6.5), (6.16), and (6.17). The propagation equation (6.5) is solved by a spectral method for paraxial propagation [33]. The paraxial evolution operator is truncated at fourth order in ΔT, and the action of the optical Hamiltonian is conveniently represented in terms of fast Fourier transforms in the radial variable. This is a fast and economical method, which avoids the difficulties associated with Hankel transform techniques. The improved QSA density equation, (6.41), is treated similarly.

The situation modeled here corresponds to conditions similar to those simulated by Andreev and co-workers [28,34]. The novel features of the present work are the demonstration of angular dependence in the Raman spectra, and the detailed calculation of phase histories. Our results show a decided angular dependence of the spectra. Our results are consistent with the experimental observations of Coverdale *et al.* [35,36] on the blueshifted part of

the spectrum. The phase information allows one to predict experimentally observed amplitude phase reconstructions of the transmitted pulse by techniques such as frequency resolved optical gating [37], which are now being used to understand laser-plasma interactions [38].

The simulation results shown below represent a laser with wavelength $\lambda=1$ μm incident on a performed plasma with density $N_e/N_c=0.002$. The paraxial parameter $\theta=0.04$, so the plasma wavelength is $\lambda_P=22.4$ μm, and the plasma length scale is $1/k_P=3.6$ μm. The propagation scale used in our general analysis is the Rayleigh range corresponding to transverse modulations on the plasma length scale, $L_R=kk_P^{-2}=80$ μm $[k_PL_R=22.4=O(1/\theta)]$, which is small compared to the Rayleigh range for the initial spot size, $L_w=\pi w^2/\lambda=1.6$ cm. The incident field is both longitudinally and transversely Gaussian:

$$a_L=a_0\exp\left[-\left[\frac{r_\perp}{w}\right]^2-\left[\frac{Z}{L_p}\right]^2\right] \tag{7.1}$$

with $w=L_p=72$ μm $(k_Pw=k_PL_p=20.1)$, and $a_0=0.27$ $(I_0=1.1\times10^{17}$ W/cm$^2)$. The longitudinal pulse coordinate $Z=z-ct$ measures the distance from the peak of the nominal (undistorted) pulse, so, for a fixed value of Z, the time coordinate $Z^0=ct$ represents the propagation distance into the plasma.

We study the development of relativistic self-focusing and wake-field generation by calculations carried out at increasing values of the propagation coordinate Z^0. Figure 7 shows the results for a propagation distance $Z^0=4$ mm $(Z^0/L_R=49.7,\ Z^0/L_w=0.24)$. Figure 7(a) shows the radial dependence of the laser intensity and the electron density, evaluated at the nominal pulse maximum $(Z=0)$. Self-focusing is indicated by a slight increase of the maximum normalized intensity $|a_L|^2$ from the incident value of 0.073 to 0.084. Further evidence is given in Fig. 7(c), which shows the radial variation in the phase. The change in sign of the curvature of the phase at the center is characteristic of self-focusing. The smooth depression in the electron density in Fig. 7(a) shows the expected expulsion of electrons from the region

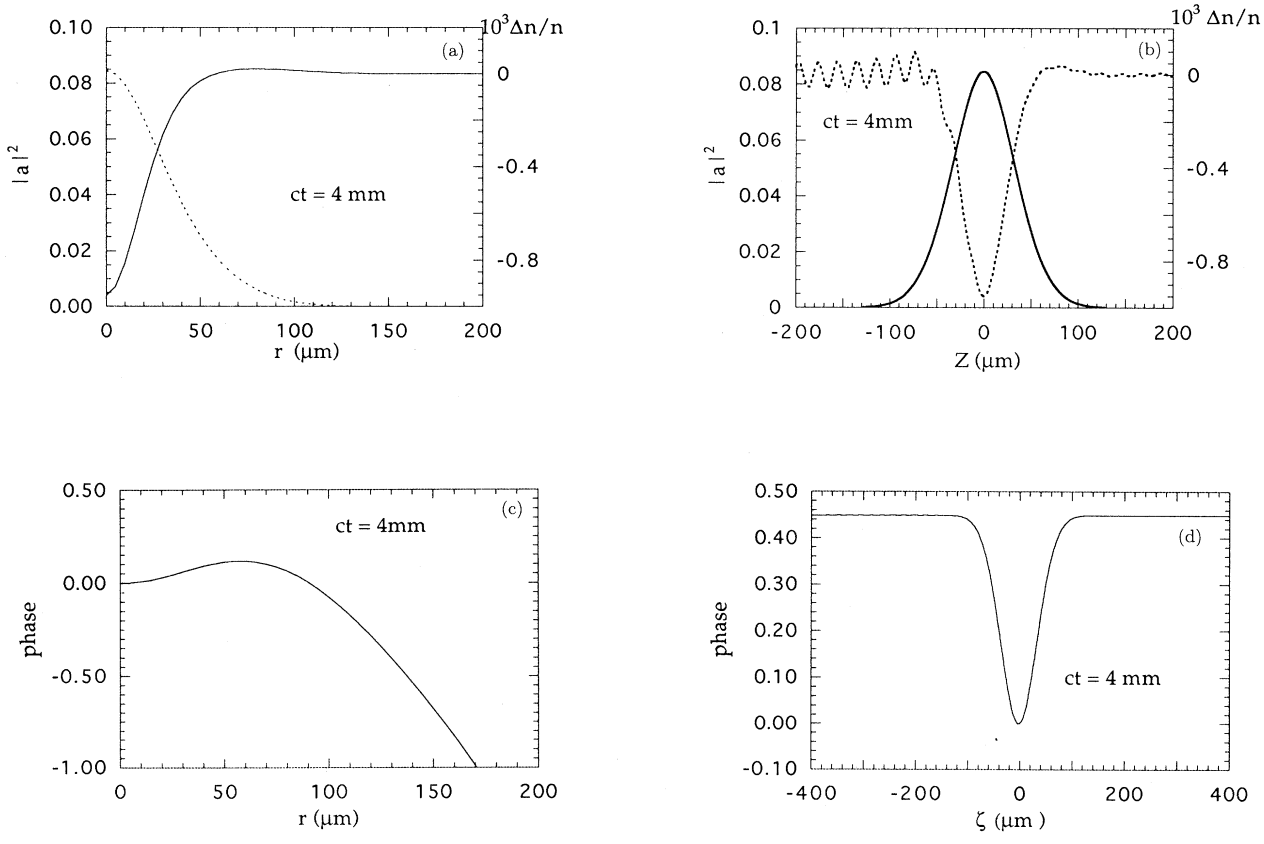

FIG. 7. Normalized intensity, phase, and electron density after propagation distance of 4 mm. (a) Radial variation of intensity (solid line, left scale) and electron density (dotted line, right scale) at $Z=0$. (b) Longitudinal variation of intensity and electron density at $r=0$. (c) Radial phase variation at $Z=0$. (d) Longitudinal phase variation at $r=0$.

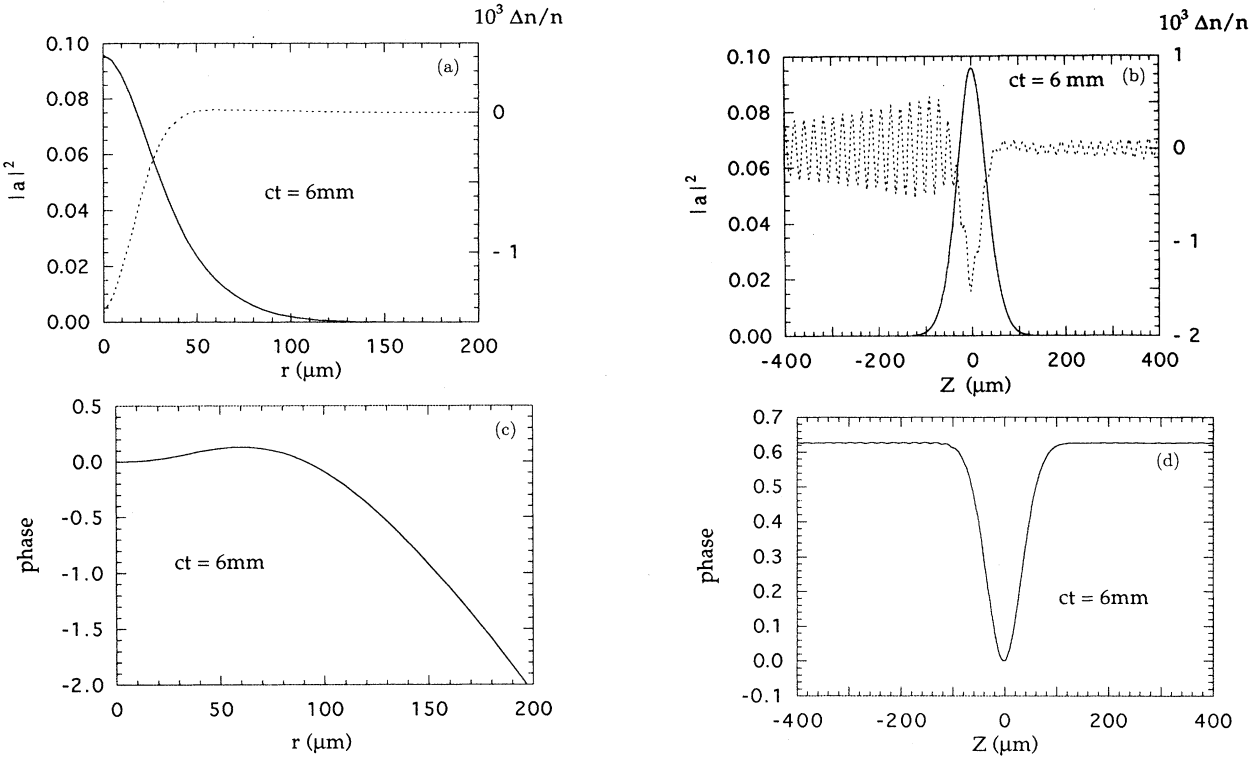

FIG. 8. Normalized intensity, phase, and electron density after propagation distance of 6 mm. Same quantities are shown as in Fig. 7.

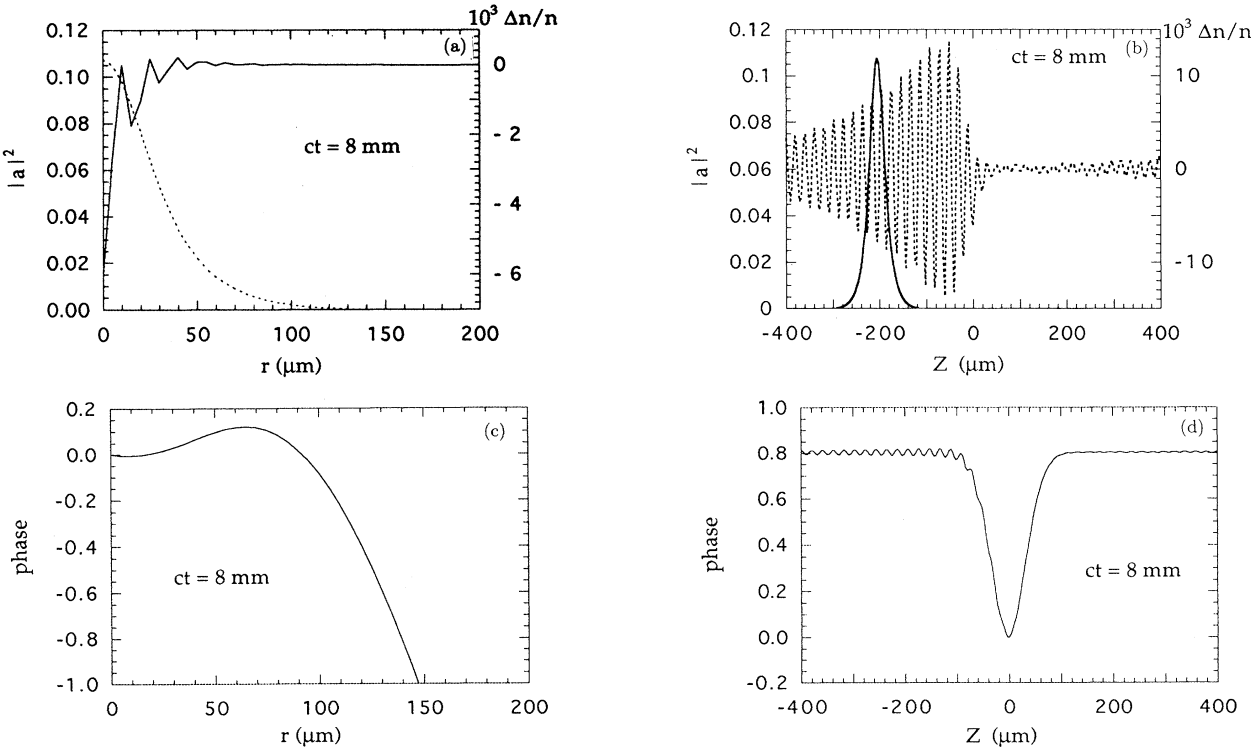

FIG. 9. Normalized intensity, phase, and electron density after propagation distance of 8 mm. Same quantities are shown as in Fig. 7.

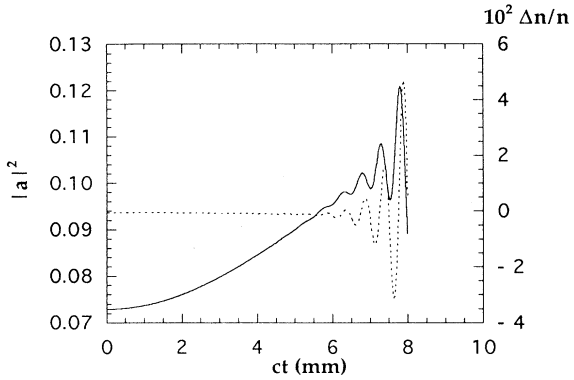

FIG 10. Axial development of normalized intensity (solid line, left scale) and electron density (dotted line, right scale) showing self-focusing and the onset of forward Raman scattering.

of highest intensity. This effect can also be seen in Fig. 7(b), which displays the on-axis intensity and density as a function of the longitudinal pulse coordinate Z. This plot also shows the large-amplitude density oscillations behind the pulse. These are wake-field oscillations at the plasma wavelength. The small-amplitude density oscillations in advance of the pulse represent aliasing effects due to the use of a finite numerical Z window. The amplitude of these spurious waves is decreased by using a window, which includes more of the wake region. In these calculations the presence of the spurious plasma oscillations in advance of the pulse had no apparent effect on the subsequent evolution of the pulse, but such effects are possible when the plasma is seeded with oscillations [34,39]. The phenomenon of self-phase modulation is seen in Fig. 7(d) which shows the on-axis laser phase as a function of Z.

Figure 8 shows the situation after propagation through $Z^0=6$ mm ($Z^0/L_R=74.51$, $Z^0/L_w=0.36$). In Fig. 8(a) the on-axis intensity has again increased, and the radial density profile shows the first evidence of transverse plasma oscillations. Increased focusing is also shown by the steepening of the radial phase profile in Fig. 8(c). The increasing importance of the wake field is demonstrated by the fourfold increase in the oscillation amplitudes as seen in Fig. 8(b), and the ripples on the phase shown in Fig. 8(d).

By the time the propagation distance of $Z^0=8$ mm ($Z^0/L_R=99.3$, $Z^0/L_w=0.48$) is reached, the laser pulse itself has been significantly affected, as shown in Fig. 9. The large transverse density oscillations seen in Fig. 9(a) have a pronounced effect on the transverse profile of the pulse; self-focusing is strongly modified so that the intensity maximum moves off-axis. This behavior has also been seen in simulations of Esarey, Krall, and Sprangle [40]. The amplitude of the wake-field oscillations, shown in Fig. 9(b), has increased fiftyfold from Fig. 8 and this has brought about deep modulations in the longitudinal pulse profile. This represents scattering of light from the plasma oscillations, usually called forward Raman scattering [9,24,28]. The same effect is represented in the strong modulation of the phase seen in Fig. 9(d). These effects can also be due to a distinct process known as self-modulation [40].

Another view of the buildup of plasma oscillations is shown in Fig. 10, which plots the central values of intensity and density versus propagation distance. Self-focusing continues until the amplitude of the density oscillations, which are strongest on-axis, is large enough to

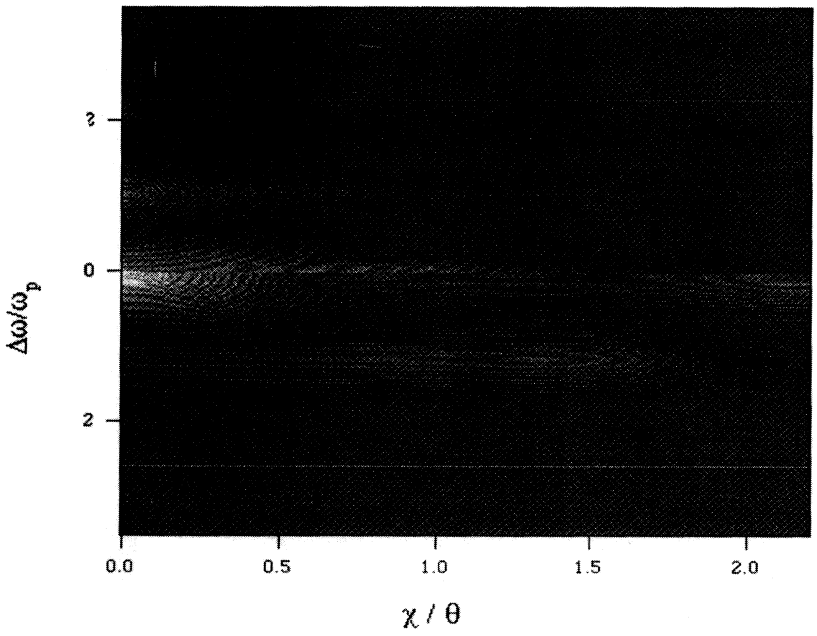

FIG. 11. Spectral density after 8 mm of propagation. Ten orders of magnitude are shown to clearly identify the angular broadening due to self-focusing and spectral broadening due to Raman scattering.

cause significant light scattering.

If the propagation distance $Z^0=8$ mm taken to be the end of the plasma, then the field radiated to infinity will be determined by the Fourier transform, $\hat{a}_L(\mathbf{q}_\perp,q_z)$, of $a_L(\mathbf{r}_\perp,z-Z^0,Z^0)$ with respect to $\mathbf{r}_\perp$ and z. Since a_L is the envelope field, the variable q_z is proportional to the shift, $\Delta\omega$, of the carrier frequency. Figure 11 shows the spectral power, $|\hat{a}_L(\mathbf{q}_\perp,q_z)|^2$, at the end of the plasma as a function of $\Delta\omega$ and the diffraction angle $\chi\approx q_\perp/k$. Two features are clearly evident. The first is the appearance of large angles (large $q_\perp$) at $\Delta\omega\approx 0$. This is a signature of self-focusing. The second feature is the generation of side bands at the Stokes and anti-Stokes frequencies for forward Raman scattering. The intensity of these side bands is exaggerated in the plot since it shows the logarithm of the spectral power. Note particularly the asymmetry between the Stokes and anti-Stokes spectra. These results suggest that angular dependence of scattered spectral power might be a useful diagnostic tool when strong wave fields are generated.

VIII. SIMPLIFIED MODELS FOR STRONG FIELDS

The weak-field limit discussed in Secs. VI and VII is not the only situation in which the general equations can be simplified. A simplified version of (5.1)–5.10) can be derived for fields of any strength provided the pulse length is very large. For short pulses the QSA equations (5.11)–(5.16) can be simplified in the case of quasiplanar pulses.

For pulse lengths that are very large compared to the plasma wavelength it is reasonable to average the full equations over the plasma-scale variables ζ and τ. If we make the additional assumption that averages of products; e.g., η, $\mathbf{p}$, all factorize, then the averaging procedure is formally equivalent to assuming a solution that is independent of ζ and τ. This assumption produces significant simplifications. The wave equation (5.5) for the wake vector potential $\mathbf{a}$ reduces to

$$\nabla_\perp^2\mathbf{a}=\eta\mathbf{p} \ . \tag{8.1}$$

Since (8.1), (5.1), and (5.4) are homogeneous in $\mathbf{p}$ and $\mathbf{a}$, the condition $\mathbf{a}=\mathbf{p}=0$ is consistent with the equations. It should be noted, however, that this condition is not imposed by the fluid equations, so its use implicitly involves the assumption that there are no instabilities in the full equations, which could asymptotically lead to nonvanishing average values for $\mathbf{a}$ and $\mathbf{p}$. The averaged form of the force equation (5.8) is the condition for equilibrium between the electrostatic and ponderomotive forces, and integration yields $\phi=\gamma-1$. The proper electron density can then be expressed in terms of γ by solving Poisson's equation (5.6) for η. With all these simplifications in force the general equations are reduced to

$$(\nabla_\perp^2+2i\partial_T)\mathbf{a}_L=\frac{n_i+\nabla_\perp^2\gamma}{\gamma}\mathbf{a}_L \ , \tag{8.2}$$

with $\gamma=\sqrt{1+\frac{1}{2}\mathbf{a}_L^*\cdot\mathbf{a}_L}$. This model has been used by several authors to study laser-induced cavitation [6,9,41]. In a future publication we will present a generalization of this model that includes ion motion.

We next consider a pulse with transverse width much larger than the pulse length or the plasma wavelength. In this situation the transverse derivatives in the QSA equations are small compared to the ζ derivatives, which refer to the plasma wavelength scale. In this limit all transverse derivatives are set to zero in (5.12)–(5.16). When this is combined with the boundary condition that all variables approach the quiescent-fluid values for large positive ζ, we find the following results: (5.12) shows that $a_z=0$, which in turn implies that the wake potential and the electrostatic potential coincide, $\psi=\phi-a_z=\phi$. (5.13) yields $\mathbf{p}_\perp=0$, and (5.16) shows that $\mathbf{a}_\perp=\mathbf{p}_\perp=\mathbf{0}$. Substituting these results into (5.11), (5.18), (5.19), and (5.23) finally yields [9]

$$(\nabla_\perp^2+2i\partial_T)\mathbf{a}_L=\frac{n_i}{1+\phi}\mathbf{a}_L \ , \tag{8.3}$$

$$\partial_\zeta^2\phi=\frac{n_i}{2}\frac{1+\frac{1}{2}\mathbf{a}_L^*\cdot\mathbf{a}_L}{(1+\phi)^2}-\frac{n_i}{2} \ . \tag{8.4}$$

IX. SUMMARY AND CONCLUSIONS

In this paper we have carried out a multiple-time-scales perturbative analysis of the coupled system consisting of Maxwell's equations and the relativistic fluid equations for the plasma electrons. The expansion parameter $\theta=\sqrt{N_0/N_c}$ is the characteristic diffraction angle for paraxial propagation, and it also defines the separation between the plasma and propagation time scales. One result of this analysis is the existence of an initial layer (temporal boundary layer) in which the fluid variables evolve from their initial quiescent values to the quasistatic limit in which the fluid is stationary in the frame moving with the pulse. The thickness of the initial layer is determined by the pulse length, so it can be a significant feature, as we shall see below. We have also shown that the quasistatic limit suffers from plane-wave instabilities that give rise to numerical difficulties, even for finite duration pulses. By combining the multiple-scale and instability analyses, we have constructed an improved quasistatic approximation that gives superior results in simulations. This scheme has a Hamiltonian structure that can also be used to constrain the behavior of the solutions.

In the weakly relativistic limit (laser intensity $I<10^{17}$ W/cm^2) we have obtained exact planar solutions and carried out simulations for cylindrically symmetric 3D pulses in order to illustrate these features. The planar solutions show that the quasistatic limit is attained after several pulse durations. The simulations exhibit relativistic self-focusing and the growth of wake-field oscillations. Transverse plasma oscillations are seen to eventually cause deep modulations in the laser pulse itself; this leads to modifications in self-focusing.

The most important experiments described by this model are related to laser wake-field acceleration or the fast igniter concept. The basic idea of the laser wake-field accelerator is that the electrons are trapped by the wake field and accelerated to the group velocity

$v_g = c(1-\omega_P^2/\omega^2)$, with energy $E/mc^2 \approx 2N_c/N_e$. Thus increasing the electron energy requires using low density plasmas. Since the optimum pulse length satisfies $L_p = O(\lambda_P) \propto 1/\sqrt{N_e}$, the required pulse length grows with energy. This implies that the transient effects illustrated in Secs. VI and VII should be taken into account, since the thickness of the initial layer is several times the pulse duration. In the fast igniter experiments the plasma density is higher, but there is no necessary relation between the pulse duration and the density, so pulses can be either short, $k_P L_p = O(1)$, or long, $k_P L_p \gg 1$. Also the total propagation distance can be comparable to the initial layer or much larger. In the first case, consideration of initial transients will be essential. In the second case, the quasistatic approximation will be satisfied for most of the propagation length, and the improved QSA can be used to suppress the instabilities described in Sec. V B.

ACKNOWLEDGMENTS

It is a pleasure to acknowledge many useful conversations with Mike Perry, Paul Bolton, Burke Ritchie, and Sam Musher. This work was performed under the auspices of the U. S. Department of Energy by the Lawrence Livermore National Laboratory under Contract No. W-7405-Eng-48.

[1] M. Tabak *et al.*, Phys. Plasmas **1**, 1626 (1994).
[2] J. Wurtele, in *Advanced Accelerator Concepts,* edited by J. S. Wurtele, AIP Conf. Proc. No. 279 (AIP, New York, 1993).
[3] C. D. Decker, W. B. Mori, and T. Katsouleas, Phys. Rev. E **50**, R3338 (1994).
[4] W. B. Mori *et al.*, Phys. Rev. Lett. **60**, 1298 (1988).
[5] T. Tajima and J. M. Dawson, Phys. Rev. Lett. **43**, 267 (1979).
[6] G.-Z. Sun *et al.*, Phys. Fluids **30**, 526 (1987).
[7] A. B. Borisov *et al.*, Phys. Rev. A **45**, 5830 (1992).
[8] T. Kurki-Suonio, P. J. Morrison, and T. Tajima, Phys. Rev. A **40**, 3230 (1989).
[9] P. Sprangle *et al.*, Phys. Rev. Lett. **69**, 2200 (1992).
[10] S. V. Bulanov *et al.*, Phys. Fluids B **4**, 1935 (1992).
[11] P. Kaw, A. Sen, and T. Katsouleas, Phys. Rev. Lett. **68**, 3172 (1992).
[12] X. L. Chen and R. N. Sudan, Phys. Fluids B **5**, 1336 (1993).
[13] B. Ritchie, Phys. Rev. E **50**, R687 (1994).
[14] W. H. Press *et al.*, *Numerical Recipes in Fortran: The Art of Scientific Computing* (Cambridge University Press, New York, 1992).
[15] N. N. Bogoliubov and Y. A. Mitropolski, *Asymptotic Methods in the Theory of Nonlinear Oscillations* (Hindustan Publishing, Delhi, India, 1961).
[16] G. Sandri, Ann. Phys. **24**, 332 (1963).
[17] L.-Y. Chen, N. Goldenfeld, and Y. Oono, Phys. Rev. Lett. **73**, 1311 (1994).
[18] Y. R. Shen, *The Principles of Nonlinear Optics* (Wiley, New York, 1984).
[19] V. Zakharov, S. Musher, and A. Rubenchik, Phys. Rep. **129**, 285 (1985).
[20] J. Kevorkian and J. D. Cole, *Perturbation Methods in Applied Mathematics* (Springer-Verlag, New York, 1981).
[21] P. Sprangle, E. Esarey, and A. Ting, Phys. Rev. A **41**, 4463 (1990).
[22] P. Sprangle, E. Esarey, and A. Ting, Phys. Rev. Lett. **64**, 2011 (1990).
[23] J. Krall *et al.*, Phys. Plasmas **1**, 1738 (1994).
[24] T. M. Antonsen and P. Mora, Phys. Fluids B **5**, 1440 (1993).
[25] C. J. McKinstrie and R. Bingham, Phys. Fluids B **4**, 2626 (1992).
[26] W. B. Mori *et al.*, Phys. Rev. Lett. **72**, 1482 (1994).
[27] J. Krall *et al.*, Phys. Rev. E **48**, 2157 (1993).
[28] N. E. Andreev *et al.*, Phys. Scr. **49**, 101 (1993).
[29] P. Sprangle, J. Krall, and E. Esarey, Phys. Rev. Lett. **73**, 3544 (1994).
[30] G. Shevets and J. Wurtele, Phys. Rev. Lett. **73**, 3540 (1994).
[31] P. Sprangle *et al.*, Appl. Phys. Lett. **53**, 2146 (1988).
[32] L. M. Gorbunov and V. I. Kirsanov, Zh. Eksp. Teor. Fiz. **93**, 509 (1987) [Sov. Phys. JETP **66**, 290 (1987)].
[33] M. D. Feit and J. A. Fleck, Opt. Lett. **14**, 662 (1989).
[34] N. E. Andreev, V. I. Kirsanov, and L. M. Gorbunov, Phys. Plasmas **2**, 2573 (1995).
[35] C. Coverdale *et al.*, Bull. Am. Phys. Soc. **39**, 1518 (1994).
[36] C. Coverdale, Phys. Rev. Lett. **74**, 4659 (1995).
[37] R. Trebino and D. J. Kane, J. Opt. Soc. Am. A **10**, 1101 (1993).
[38] P. R. Bolton *et al.*, J. Opt. Soc. Am. B (to be published).
[39] D. Fisher and T. Tajima, Bull. Am. Phys. Soc. **39**, 1732 (1994).
[40] E. Esarey, J. Krall, and P. Sprangle, Phys. Rev. Lett. **72**, 2887 (1994).
[41] A. B. Borisov *et al.*, Phys. Rev. Lett. **68**, 2309 (1992).

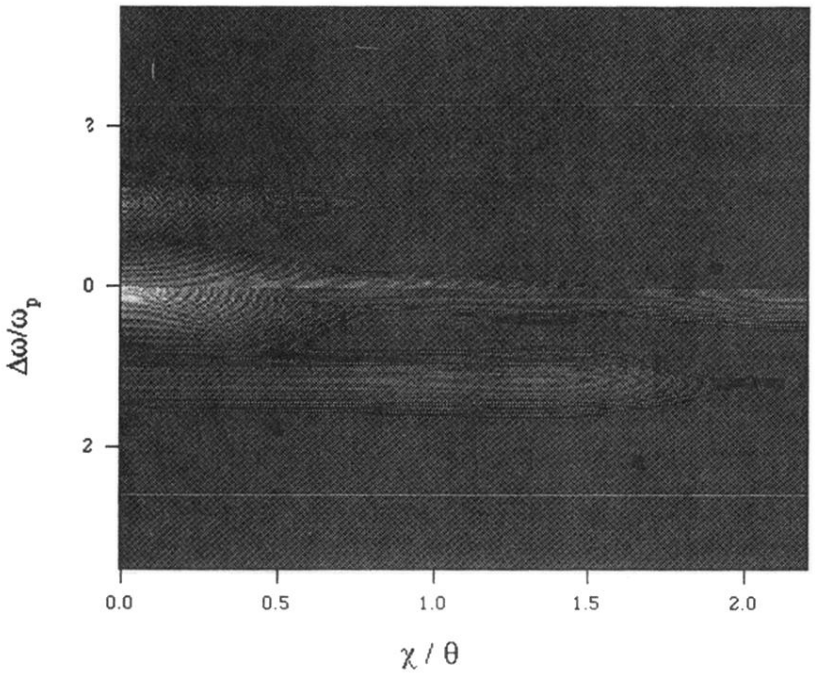

FIG. 11. Spectral density after 8 mm of propagation. Ten orders of magnitude are shown to clearly identify the angular broadening due to self-focusing and spectral broadening due to Raman scattering.